NUCLEAR FUEL (OXIDE) CLAD THERMIONIC CONVERTERS

QUARTERLY TECHNICAL PROGRESS REPORT

FOR THE PERIOD

MAY 1 THROUGH JULY 31, 1963

Contract AF33(657)-10077
Project Number: 8173
Task Number: 817305-20

Prepared for:

Aeronautical Systems Division
Air Force Systems Command
U. S. Air Force
Wright-Patterson Air Force Base, Ohio

Prepared by:

Martin Marietta Corporation
Nuclear Division
Baltimore 3, Maryland

August 15, 1963

MND-2945 3

DISCLAIMER

The work covered by this report was accomplished under Air Force Contract AF33(657)-10077, but this report is being published and distributed prior to Air Force review. The publication of this report, therefore, does not constitute approval by the Air Force of the findings or conclusions contained herein. It is published for the exchange and stimulation of ideas.

INTRODUCTION

This program, Nuclear Fuel (Oxide) Clad Thermionic Converters, Contract AF33(657)-10077, encompasses the fabrication, performance testing, and evaluation of a double diode thermionic converter containing fuel-bearing emitters. In a parallel effort, fuel pellets, with dimensions comparable to those of the emitters, are to be fabricated, thermally endurance tested, and evaluated. Finally, the results of the preceding efforts will be utilized to accomplish the design of an improved thermionic converter.

This is the third Quarterly Technical Progress Report submitted under this program. It describes the technical progress achieved during the period of May 1 through July 31, 1963.

SUMMARY

PRESENT WORK

Fabrication of the components for the FDM-1 converter and its back-up device was completed. The FDM-1 converter was assembled and preparations for testing were completed. Performance testing was initiated and a total of 330 hours of operation at temperatures above 1000°K in a cesium environment were logged by the end of the quarterly period. During this time the peak emitter temperature reached was approximately 2000°K with a thermionic output of nearly 2 watts/cm^2. Toward the end of the reporting period, indications of a cesium leak were observed and the device was shut down for examination.

A 500 hour thermal endurance test of the clad fuel pellets was performed. A post-test examination was conducted and no diffusion of UO_2 into the cladding was observed. A thermal conductivity test specimen was exposed to a temperature of 1550°C for 500 hours with the result that some intergranular diffusion was noted. The post-test examination of the vacuum emission test pellet was also completed.

The design of the advanced double diode thermionic converter utilizing the results of prior efforts was initiated.

FUTURE WORK

During the next quarterly period, the FDM-1 converter will be examined to determine if a design change is neccessary and/or appropriate repair possible. Components for the back-up device (FDM-2) will be suitably modified and assembled, if required, and testing resumed. Converter performance data will be evaluated and a detailed examination performed at the conclusion of testing.

The design of the advanced double diode thermionic converter will be completed.

A Final Technical Report describing all work accomplished under this program will be prepared in draft form.

TECHNICAL DISCUSSION

I. Fabrication of the Fueled Clad Double Diode Thermionic Converter

A. Fabrication of Converter Components

Fabrication of components for the FDM-1 converter and its back-up device began in January 1963. Prior knowledge and experience gained from the fabrication and assembly of Martin-sponsored devices were utilized to the fullest extent and proved invaluable.

Details of some of the procedures that were necessary for the fabrication of several complex components for the FDM-1 converter are as follows:

Inner Anode Assembly

Arc cast columbium bar stock was rough machined and subsequently vacuum annealed to remove machining stresses. The inside diameter was machined to final dimensions. One end of the tube was counterbored to accept the columbium back-emission shield and the tantalum-10% tungsten center-lead.

Both the back-emission shield and the center-lead were formed by pressing a male die into suitable, annealed sheet stock backed up by a lead block. This technique was found to give excellent formability to the above refractory metals.

Following machining of the outside diameter, the back-emission shield (0.020" thick) and the center-lead (0.010" thick) were located in the anode tube counterbore (0.025" deep). The anode tube was positioned on a holding chill, with provisions for holding a pin and weight, and was weld-brazed in the remote chamber.

Twelve equi-spaced cesium passage holes were drilled through the back-emission shield and center-lead adjacent to the wall of the anode tube. The previous weld-braze resulted in a slight growth on the anode tube outside diameter which was machined off.

The outside surface of the tube was carefully grit blasted in preparation for an Al_2O_3 flame spray which was subsequently applied to a thickness of about 0.015". The flame spray was ground between centers to provide about 0.0005" clearance for assembly into the threaded container assembly. Final machining operations involved cutting to length and reboring the annulus in the center lead to finished dimensions.

Threaded Container Assembly

Arc-cast columbium bar stock was rough machined and subsequently vacuum annealed to remove machining stresses. The ends of the container were machined to accept the tantalum flange washers. At the same time, the cesium inlet tube hole was bored through the wall of the container. The columbium cesium inlet tube was welded to the container as a dry box operation. Next, the flanges were weld-brazed to the ends of the container in the remote chamber. A flame-sprayed layer of Al_2O_3 was applied to the appropriately grit blasted external surface of the container. By performing the welding, weld-brazing and flame-spraying at this stage in the manufacture, it was possible to compensate for the distortion resulting from these operations.

Considerable effort was expended in the final machining of the threaded container assembly. The requirements of close tolerances and a 2 RMS interior surface finish necessitated precise machining. Numerous special jigs, fixtures and gages were required.

Other Converter Components

The balance of the converter components was fabricated by more or less routine and established techniques. A photograph of the completed components and assemblies is shown in Figure 1.

All welding, brazing or weld-brazing employed in the manufacture of the FDM-1 converter components or assembly were performed in a remote automatic chamber or a dry box. In each case, the container was evacuated to 50 microns or less and back-filled with 99.9995% welding grade Argon for a total of three times prior to performing the joining operation under a positive pressure of Argon.

All parts were degreased, chemically etched and not physically handled prior to joining. Every effort was exerted to achieve and maintain maximum cleanliness. Where applicable, joined components were mass spectrometer leak tested to 10^{-8} cc/sec or better and/or gammagraphed to insure integrity.

Internal ceramic components with the exception of the finished inner anode assembly were vacuum outgassed at 1500°C for one hour. It was not considered practical to outgas the inner anode assembly because of the design limitations of the 0.0005" fit.

All finished components were subjected to a complete quality control inspection and complete written reports were maintained. Components not conforming to specifications were rejected, except in cases in which it was certain the deviation would not affect the intended function.

B. Assembly of Converter Components

The initial step in the assembly of the FDM-1 converter was to determine the axial location of the top collar relative to the top cathode. It was necessary to construct a positioning jig to assure the alignment of the bottom edge of the top cathode emitter to the edge of its respective collector. The various components were assembled over the jig, compressed to remove all clearance and the location determined as seen in Figure 2.

Following location, the columbium braze filler was positioned between the top cathode and the top collar and brazed using the TIG technique in the automatic remote chamber with the aid of various fixtures and chills as seen in Figure 3.

A ceramic-to-metal seal and weld filler shim were positioned over the top cathode-top collar subassembly. Precision copper blocks were attached to the flanges by means of three clamps with integral set-screws. These blocks served a twofold purpose: precise alignment of components, and adequate chill technique for welding. It was necessary to split and pin the lower chill block for location around the ceramic-to-metal seal.

The fixtured assembly was positioned in the remote welding chamber as seen in Figure 4. TIG fusion welds were made on the mating flanges at non-interfering locations. The chamber was opened with the three clamps being relocated to the welded positions subsequent to making the final three welds.

The completed inner anode assembly was positioned inside the threaded container. The prior subassembly with its accompanying weld filler shim and the upper alignment insulator was inserted into the threaded container so that the end of the cathode fit into the hole of the center lead. The end of the cathode was flared over and around the center lead by exerting force on a punch supported by an anvil extending into the top cathode annulus.

The lower flanges of the top cathode were welded by a similar procedure as described for the upper flanges. It was necessary, however, in this case to use two pinned chill blocks. The fixtured assembly before welding is seen in Figure 5. The resulting assembly was mass spectrometer leak tested to confirm vacuum integrity.

The bottom cathode with the lower alignment insulator and the center-lead spacer was positioned and locked inside the previous assembly by means of a threaded lock nut. The lock nut was first securely tightened and then backed off to give 0.020 inch axial clearance. The assembly seen in Figure 6 was gammagraphed to assure the proper inner arrangement.

The bottom collar was welded to another ceramic-to-metal seal in the remote chamber. This subassembly and weld filler shim were located on the bottom cathode. The bottom cathode upper flanges were maintained in position by three small spring clips as seen in Figure 7. The assembly was mounted on a motor driven turntable with the torch independently held so as to approximate the conditions of the remote chamber. The clamp and wire attached to the device were used to establish a suitable electrical ground.

The bottom ceramic-to-metal seal flange to the bottom threaded container flange was welded by the previously discussed method in the remote chamber. Figure 8 is a view of the assembly with the alignment chill blocks and clamps in place in the remote chamber just prior to welding.

After completing the above weld, the device as pictured in Figure 9 was leak tested to confirm vacuum tightness and gammagraphed three times at 120° intervals. Positive prints of these gammagraphs may be seen in Figures 10, 11, and 12.

Following the leak test and gammagraphs, the cesium supply assembly, Figure 13, previously fabricated, was clamped to the prior assembly as seen in Figure 14 and welded in the dry box.

The completed FDM-1 converter, shown in Figure 15, was given a final mass spectrometer leak test. The results of this test and all prior tests were affirmative with no detectable leak at a rate of 10^{-8} cc/sec.

Four platinum-platinum, 10% rhodium thermocouples to monitor the anode temperatures were resistance spot welded to the external surface of the threaded container after first carefully removing a small area of the insulating Al_2O_3 layer. These couples were located to correspond to the previously prepared grooves on the internal diameter of the split thermal sleeve which was then positioned in its proper location around the threaded container of the device as seen in Figure 16.

Two optical temperature viewing sleeves were positioned in each of the cathode assemblies with the aid of special tools as seen in Figure 17. The assembly was positioned into the anode temperature control and instrumentation housing as seen in Figure 18. Final assembly in preparation for instrumentation and test involved the installation of the upper and lower containers, output leads and external vacuum plumbing.

II. Performance Testing of the FDM-1 Converter

A. Pre-Test Preparations

The FDM-1 converter was delivered to the Energy Conversion Laboratories by the end of May completely assembled and gammagraphed. The geometry of the device satisfied design requirements at the time in that the emitters were well centered within their cylindrical collectors.

The device was instrumented and installed in the vacuum test chamber for evacuation and bake-out. Several minor vacuum leaks in the test chamber delayed the initial bake-out period. After 50 hours of outgassing time (up to temperatures of 1600°K), it was noted that Diode #1* would intermittently short-circuit internally, depending primarily on temperature changes in the emitter. Also, in a cold condition, there was an excessive amount of play in the emitter of Diode #1 evidenced by readily caused open- and short- circuit conditions when force was applied on the emitter lead and seal.

The module was removed from the vacuum test envelope and gammagraphed. Careful comparison of this gammagraph with those previously taken showed that the emitter of Diode #1 was not located properly and that its alignment pin was not located in the center alignment ceramic. This permitted the emitter to move sideways due to thermal expansions and cause the diode to short-out electrically. It was determined that the condition could only be remedied by disassembly.

The disassembly was accomplished by cutting the weld between the emitter lead and the seal flange of Diode #1 and removing the seal by cutting off the edge weld of the seal flange nearest the collector. All components removed (emitter, center ceramic spacer, and seal) appeared to be in excellent condition with no evidence of surface discoloration or alteration.

---

*The left-hand diode shown in Martin drawing 390-0790116, reproduced in the previous Quarterly Technical Progress Report, is designated as Diode #1. The right-hand diode is designated as Diode #2.

Examination revealed that the retaining ring which provides for the final location of the emitter of Diode #1 was backed-out excessively (two turns, ~ 0.040") and allowed the emitter locating pin to slip out of the center ceramic spacer. It is uncertain as to whether this ring worked out these two turns during the assembly process or was inadvertently located in reference to a "false bottom" during the installation procedure.

Since all components were still in excellent condition, the device was reassembled. A locating tab (fabricated into the closing seal flange welds) was added to prevent accidental turning of the retaining ring.

Following reassembly, the converter was again subjected to the evacuation and outgassing process. Behavior of the modules looked normal and the vacuum characteristic curves, obtained with an AC sweep voltage displayed on an oscilloscope, possessed the classical shape for vacuum diodes.

After 113 hours of outgassing (including the 50 hours prior to the disassembly discussed above) at pressures of 6×10^{-7} mm Hg while the emitter temperatures (T_E) were at 2000°K, the device was cooled down for the crimp-off operation. After breaking the cesium ampule (with the device cold and at a pressure of 8×10^{-8} mm, read at the ion gauge), the module was valved off and crimped-shut twice with each crimp seam-welded. The final distillation of cesium from the glass ampule container into the water-cooled cesium reservoir was carried out and the ampule section removed. By early July, the FDM-1 was operated as a cesium plasma thermionic converter.

B. Performance Testing

After cesium distillation, the FDM-1 converter was operated for 330 hours of which approximately 150 hours were at conditions to produce greater than 1 w/cm^2 from the nominal 15 cm^2 area of each emitter. For approximately 5 hours of this time, the device produced nearly 2 w/cm^2.

During the outgassing period and initial operation with cesium vapor, emitter temperature calibration data (shown in Figure 19) were obtained. While the glass viewing plates were clear, measurements of emitter temperature (optical pyrometer - Leeds and Northrup at 0.06 u) as seen by means of the sight ring holes were taken and plotted against total power input into each diode. It must be understood that these are the temperatures of the sight ring-emitter inner wall at the center of the emitter and are not the actual emitter surface temperatures over the entire emitting surface. The actual emitter temperature profile may show a 50 to 100°K drop near each end.

It has been found in the past that such a curve does give good consistency between runs and is a good indication of variations in operating conditions. Actual emitter surface temperatures are quite difficult to obtain with accuracy in the cylindrical configuration. For the conditions of measurement (utilizing a calibrated optical pyrometer sighting into a reasonable "black body" sight hole) the temperature of that area of the emitter is believed to have an accuracy of ± 50°K.

There is no obvious reason why the same power input density should produce higher emitter temperatures in FDM-1 than in Test II-2.* Several speculations do exist, however, that (1) the FDM-1 collector temperature was purposely made hotter (based on prior experience obtained during the testing of the Test II-2 device, a higher collector temperature appeared desirable for improved performance), and 2) smaller thermal conductivity of the UO_2 molybdenum cermet might produce a higher emitter sight-hole temperature for a lower power input density.

Temperatures and cesium pressure in the FDM-1 were raised gradually and device performance was normal. Figure 20 shows one of the early output characteristic curves obtained from FDM-1. Maximum power output is seen to be about 1 w/cm^2 at $T_E \simeq$ 1640°K (obtained from Figure 19, and optical pyrometer readings).

*Test II-2 is a double module converter of the same design and electrode materials as the FDM-1, but with 12.5 cm^2 emitters and no UO_2 fuel. It is operated under a Martin-sponsored program. For detailed test results, see Martin report MNI-CRP-3067, Compact Reactor Program Quarterly Progress Report, Number X. April through June, 1963.

By the middle of July, the FDM-1 converter was operated at its highest temperature to date and these results are shown in Figure 21. Here device performance is nearly 2 w/cm^2 and, if internal power losses were considered, the power output of the individual diodes would be well over 2 w/cm^2. These curves compare favorably with Test II-2 data as shown in Table I.

TABLE I

Comparison of the Outputs for the FDM-1 and Test II-2 Converters

	Diode #	T_{Cs} °K	T_E °K	P_o w/cm^2	I_o a/cm^2	V_o volt
FDM-1	1	570	2000	1.7	2.85	0.60
Test II-2	1	570	1940	1.93	3.0	0.63
FDM-1	2	570	1940	1.83	3.7	0.50
Test II-2	2	570	1900	1.54	2.8	0.55

The above data according to Test II-2 curves are not at the optimum cesium temperature (T_{Cs}). For these values of T_E, the T_{Cs} should have been optimum at about 575°K.

From the very beginning of operation of FDM-1, it has been noted that open circuit voltages have been quite high (close to 2 v). This is the first device (double module type) which has employed a back emission shield and center lead structure which was designed to reduce the losses of Diode #1. This could account for the larger open circuit voltages for Diode #1. The increase in Diode #2 open circuit voltage is probably due to surface effects.

The back emission shield has apparently eliminated to a large extent the power loss observed in the first double module (the Martin Test II device).*

* Details of the operation and test results of the Test II device are given in Martin report MND-TDR-4537, "Compact Reactor Program Quarterly Progress Report" Number VIII October through December, 1962

and no further change in the intermodular region is indicated at this time. However, the cesium vapor passage holes still present line-of-sight passage for electrons from one emitter and gap to the other. For a further improvement in efficiency, the holes on the intermodular lead should be offset from those on the back-emission shield.

In the FDM-1, as discussed previously, some effort was made to provide higher collector temperatures in both diodes. This involved removing about 0.003" from the outer diameter of the inner copper coolant sleeve. There is a possibility that this may have had the effect of increasing the open circuit voltage generated in each diode.

Figures 22 and 23 are plots of output voltages vs T_{C_3} with output current as a parameter. These plots were obtained from photographs of the AC sweep characteristics of each diode with the AC sweep being applied to the series connection. Figures 22 and 23 have the appearance of a normally operating diode. Also shown on these figures are curves of constant output power.

During operation, the characteristic output curves were observed while changes were made in the collector temperature. The FDM-1 employed the helium pressure envelope type of collector temperature control. This mechanism for control of the contact resistance between the coolant and the collector permitted a maximum change on the external collector surface of about 50°K. This amount of change in collector temperature (T_C) did show that the T_C with a vacuum in the envelope (lowest effective cooling path obtainable) is still lower than optimum. However, since output changes were slight, the departure from optimum should be minimal. The design as it exists will permit optimization of T_C as the output power is increased to the range of 5 to 7 w/cm^2.

Further analysis will be made of the performance characteristics observed during unbalanced and off-optimum operating conditions and the results will be included in the final technical report.

[illegible] were made [illegible] [illegible] FM-1 [illegible] operat[illegible] [illegible] was also operated at [illegible] output power levels [illegible] efficiency was approximately [illegible]% [illegible] output power the efficiency was [illegible]% [illegible] with the same electrode materials [illegible] approximately the same total area have demonstrated [illegible]% efficiencies for similar operating conditions. The reason for the differences in observed efficiencies is probably related to intermodule lead heat conduction losses, [illegible]-emission losses, and end effects. Of course the end losses inherent with electrical heaters are eliminated in actual nuclear application.

[illegible] hours of cesium vapor operation, the odor of cesium [illegible] detected when the vacuum test envelope of [illegible] was opened. An inspection of the module, however, did not indicate the presence of a leak. The device was [illegible] operated over a weekend and after 190 hours of operation a deposit appeared on the viewing glass of the [illegible] diode. When air was introduced into the vacuum chamber, the material deposited on the glass was found to hydrolize into an oily liquid. A spectrographic analysis and chemical tests confirmed that cesium was present. Operation of the device after this produced a slow deterioration in performance probably coupled with the slow loss of cesium.

The FM-1 converter had a total of 330 hours operation as a cesium converter. The temperature history of the individual emitters is summarized in Figure 2[illegible]. In the diagram the hours at 1000°K indicate that time during which only the filaments were energized and the emitters were heated by radiation only. The upper plot shows the temperature profile during the outgas period and includes an estimated [illegible] thermal cycles to a room temperature condition. The lower plot is a continuation and shows the profile of temperature during cesium vapor operation. Here the converter was cycled 15 times to room temperature. These cycles are the result of burned out bombardment filaments, filaments in poor alignment, etc.

The FM-1 will now be examined to determine the location and cause of the cesium leak. It appears to be located where the lower seal support flange is welded to the emitter [illegible]. [illegible] investigation will be

conducted to determine if an error exists in the design. The emitter of Diode #1 will be removed to examine the internal structure. If it is in a condition suitable for repair, repair will be performed and the device will be re-evaluated and recharged with cesium. On the other hand, if no inherent faults are found in the present design and repair is not appropriate, the detail components for the back-up device (FDM-2) will be assembled and made ready for testing. In this case, detailed analysis and examination of the FDM-1 will be performed.

The important conclusions of the FDM-1 performance tests to date are:

a. The series operation of thermionic diodes in a common cesium environment is feasible. In addition, the performance resulting from such a mode of operation is comparable to the cumulative performance observed from two single diodes operated individually.

b. No significant difference in thermionic performance has been observed between fueled and unfueled double module converters.

C Plans for the Next Quarterly Period

An examination of the FDM-1 converter will be performed to determine if a design change is necessary and/or appropriate repair possible. Components for the back-up device (FDM-2) will be suitably modified and assembled if required and testing resumed. Converter performance data will be evaluated and a detailed examination performed at the conclusion of testing.

III Evaluation of Clad Fuel Pellets

A. Thermal Endurance Test

Prior to thermal endurance testing the previously fabricated pellets were first individually sealed in a tungsten capsule containing an argon atmosphere. Each tungsten capsule was in turn sealed in a tantalum capsule that also contained an argon atmosphere. The double container technique was used to ensure complete isolation of the test pellets from the furnace atmosphere. The furnace used for the thermal endurance test was of a graphite resistance-type with a dynamic argon atmosphere. It is not general procedure to take such elaborate precautions to prevent carbonization of refractory metals in this furnace for normal development or production work, but the encapsulation described above was considered highly advisable in view of the long dwell time at temperature and the nature of the work.

The encapsulated pellets were stacked in an open end graphite boat with their long axis horizontal The pellets were located in such a manner to permit utilization of the normal temperature gradient in the furnace to give thermal endurance data at several different temperatures. Direct temperature readings, taken three times a day with a micro-optical pyrometer, showed temperatures of 1550, 1500, 1450 and 1340°C for four of the pellets, while the two remaining pellets were estimated to have been between 1450 and 1500°C. The endurance test was run for 500.5 hours at equilibrium. By mutual agreement the thermal endurance test was run for 500 hours instead of the originally scheduled 200 hours in order to duplicate the planned fueled double diode operating time and to increase the value of the materials compatibility data obtained.

B. Post-Thermal Endurance Test Examination

1. Thermal Conductivity

Figure 25 shows the thermal conductivity vs. temperature curves for the thermal conductivity specimens both before and after the thermal endurance test compared to the thermal conductivity of pure

molybdenum and sintered uranium dioxide. The spread between the two curves is not significant when the general precision of thermal conductivity measurements is considered. However, the slightly higher thermal conductivity of the pellets after the thermal endurance test could be attributed to sintering and grain growth in the matrix of the cermet. The significant factor in this phase of the work is the fact that the thermal conductivity does not decrease with exposure to high temperatures for extended periods. A decrease in thermal conductivity with increasing operating time would act to further increase the centerline temperature of the fuel, and increase the amount of fission gas release in a reactor environment.

2. Electrical Resistivity

The thermal conductivity test specimens were also used as test specimens for the determination of electrical resistivity. The electrical resistivity was measured on each pellet, both before and after the thermal endurance test. Each pellet was clamped between copper bars, and a current was passed through the pellet. Tungsten probes were used to measure the potential drop across a measured length of the pellet. The results of these measurements are presented in Table II.

These experimentally determined resistivity values all fall within a factor of ten of the published value for pure molybdenum (5.7×10^{-6} ohm-cm). It appears that, as in the case of thermal conductivity, the molybdenum in the matrix of the cermet makes a significant contribution to electrical conductivity. The fact that the variation in resistivity with metering current was smaller after the thermal endurance test is again indicative of sintering of the molybdenum in the matrix of the cermet

3. Hardness Values of the Cladding

The before and after thermal endurance hardness values do not reveal any precise quantitative data due to the rather large variations in readings on each discrete pellet. In general, the variation in hardness was much greater

TABLE II

ELECTRICAL RESISTIVITY PRIOR TO THERMAL ENDURANCE TESTING

	I(amps)	ΔV(mv)	R(ohms)	ρ(ohm-cm)
Sample I	7.83	0.28	3.58×10^{-5}	6.31×10^{-5}
	2.41	0.058	2.41×10^{-5}	4.24×10^{-5}
	1.26	0.022	1.75×10^{-5}	3.08×10^{-5}
Sample II	8.85	0.297	3.36×10^{-5}	6.02×10^{-5}
	1.22	0.027	2.21×10^{-5}	3.95×10^{-5}
	0.86	0.014	1.63×10^{-5}	2.91×10^{-5}

ELECTRICAL RESISTIVITY AFTER THERMAL ENDURANCE TESTING

	I(amps)	ΔV(mv)	R(ohms)	ρ(ohm-cm)
Sample I	8.80	0.280	3.18×10^{-5}	5.76×10^{-5}
	2.38	0.076	3.19×10^{-5}	5.78×10^{-5}
	1.00	0.034	3.40×10^{-5}	6.16×10^{-5}
Sample II	8.95	0.200	2.23×10^{-5}	4.10×10^{-5}
	2.40	0.062	2.58×10^{-5}	4.74×10^{-5}
	1.00	0.026	2.60×10^{-5}	4.78×10^{-5}

after the thermal endurance test and usually was much greater than the average change in hardness. The results of the test, shown in Table III, do indicate that the hardness of the cladding is decreasing as the amount of recrystallization increases. The data are not sufficiently precise to warrant further deductions.

4. Dimensional Stability

The thermal endurance test pellets were indexed with a series of microhardness bench marks in such a manner that three diametrical measurements were made at the center and each end of the pellet. The bench mark system is illustrated in Figure 26. The measured dimensions of the test pellets are shown in Tables IV and V and their visual appearance is presented in Table VI. The data indicate that the dimensional stability of the pellets was good.

5. Materials Compatibility

All of the thermal endurance test pellets and the thermal conductivity samples were sectioned, metallographically mounted and polished for materials compatibility evaluation. The combination of the thermal endurance test specimen, the thermal conductivity test specimen, the vacuum emission test pellet, and the fueled thermionic emitters will provide materials compatibility data over the temperature range 1340°C to 1670°C upon completion of the program

None of the thermal endurance test specimens showed any evidence of diffusion of the uranium dioxide through the molybdenum-1/2% titanium alloy cladding. The temperature range covered by these pellets ran from 1340 to 1500°C. Photomicrographs of a typical cladding-fuel interface of each of these pellets are shown in Figures 27 through 31. Definite evidence of diffusion of uranium dioxide into the molybdenum-1/2% titanium alloy cladding was observed in the thermal conductivity specimens that were exposed to a temperature of 1550°C during the 5000 hour thermal endurance test. Figures 32 and 33 are representative photomicrographs of areas of the fuel-cladding interface of these pellets and illustrate that the observed diffusion is very similar in nature

TABLE III

Microhardness values of the thermal endurance pellets before and after the thermal endurance test - all hardness values are in Rockwell B scale.

Specimen	Endurance Test Temperature	Hardness Values Position on Pellet* 1	2	3	Maximum Variation	Mean Hardness Value	Change in Mean Hardness Value
147-2	Pre-endurance	79	80.7	81.5	2.5	80.4	
	1340°C	89	78	75.5	13.5	80.8	+0.4
147-4	Pre-endurance	82.2	81.7	83.2	1.5	82.4	
	1400°C	75.0	69.0	77.5	8.5	73.8	-8.6
147-7	Pre-endurance	87.8	86.7	85.5	2.3	86.7	
	1450 - 1500°C	83.5	83.5	82.5	1.0	83.2	-3.5
147-9	Pre-endurance	84.2	86.0	85.5	1.8	85.2	
	1450 - 1500°C	69.0	77.5	84.0	15.0	76.8	-8.4
147-10	Pre-endurance	87.8	86.2	80.7	7.1	84.9	
	1500°C	62.0	76.5	77.0	15.0	71.8	-13.1

* See Figure 26 for position locations.

TABLE IV

Pre-and Post-Test Dimensions of Thermal Endurance Test Pellets

Specimen	Endurance Test Temperature	Position (O'Clock)	Diameter Measurements, inches 1	2	3	Average
147-2	Pre-test Values	12	.5050	.5049	.5049	.5049
		4	.5048	.5049	.5048	.5048
		8	.5049	.5049	.5050	.5049
		Average	.5049	.5049	.5049	
147-2	1340°C	12	.5050	.5043	.5043	.5045
		4	.5047	.5044	.5043	.5045
		8	5050	.5045	.5045	.5047
		Average	.5049	.5044	.5044	
147-4	Pre-test Values	12	.5050	.5050	.5050	.5050
		4	.5050	.5050	.5050	.5050
		8	.5050	.5050	.5050	.5050
		Average	.5050	.5050	.5050	
147-4	1400°C	12	.5050	.5050	.5085*	.5062
		4	.5050	.5050	.5050	.5050
		8	.5050	.5050	.5050	.5050
		Average	.5050	.5050	.5062	
147-7	Pre-test Values	12	.5049	.5050	.5050	.5050
		4	.5049	.5049	.5049	.5049
		8	.5049	.5050	.5050	.5050
		Average	.5049	.5050	.5050	
147-7	1450 - 1500°C	12	.5049	.5050	.5048	.5049
		4	.5049	.5049	.5049	.5049
		8	.5049	.5050	.5050	.5050
		Average	.5049	.5050	.5049	

TABLE IV - CONTINUED

Specimen	Endurance Test Temperature	Position (0° Clock)	Diameter Measurements inches 1	2	3	Average
147-	Pre-test Values	12	.5050	.5050	.5049	.5050
		4	.5050	.5050	.5050	.5050
		8	.5050	.5050	.5050	.5050
		Average	.5050	.5050	.5050	
147-9	1450 - 1500°C	12	.5050	.5050	.5049	.5050
		4	.5050	.5050	.5050	.5050
		8	.5050	.5050	.5050	.5050
		Average	.5050	.5050	.5050	
147-10	Pre-test Values	12	.5050	.5050	.5050	.5050
		4	.5049	.5050	.5050	.5050
		8	.5050	.5049	.5049	.5049
		Average	.5050	.5050	.5050	
147-10	1500°C	12	.5067	.5050	.5050	.5056
		4	.5064	.5050	.5050	.5055
		8	.5060	.5049	.5060	.5056
		Average	.5064	.5050	.5053	

... stuck to tungsten container. The isolated high reading for the diameter of specimen ... an area where the pellet stuck to the tungsten capsule

TABLE V

Pre-and Post-Test Lengths of Thermal Endurance Test Pellets

Specimen	Pre-Test Length, In.	Endurance Temperature, °C	Post-Test Length, In.
147-2	1.394	1340	1.394
147-4	1.420	1400	1.422
147-7	1.318	1450 - 1500	1.319
147-9	1.362	1450 - 1500	1.364
147-10	1.354	1500	1.355

TABLE VI

Post-Test Visual Appearance of Thermal Endurance Test Pellets

Specimen	Endurance Temperature, °C	Visual Appearance
147-2	1340	Bright with no visual changes. No large grains evident.
147-4	1400	Bright, some dull spots due to the pellets adhering to the tungsten capsule. Some grain boundaries visible.
147-7	1450 - 1500	Bright with no visual defects, no grain boundaries visible.
147-9	1450 - 1500	Bright, some grain boundaries visible.
147-10	1500	Bright, one small dull spot on end cap and side of pellet from adhering to tungsten capsule. Surface showed a fair amount of grain boundaries.

to that observed in the vacuum emission test pellet reported in the previous quarterly report. The observed diffusion in the cladding of these pellets differed from that observed in the vacuum emission test pellet in that it was evenly distributed with respect to location and, in some cases, had penetrated the full 5 mils of cladding. The diffusion previously observed in the vacuum emission test pellet, conversely, appeared to occur preferentially with respect to location. This difference in uniformity of diffusion appears to be related to the temperature distribution during testing. For the thermal conductivity specimens, a fairly uniform temperature distribution was maintained whereas, in the case of the vacuum emission test pellet, temperature gradients were present (See Figure 34).

Several important factors must be considered before acceptance of the observed diffusion of uranium dioxide through the molybdenum-1/2% titanium alloy can be accepted as a virtual certainty. The first factor is the stoichiometry of the uranium dioxide in the starting fuel form system. No precise quantitative analysis was run on the starting material to determine the exact oxygen content. The stoichiometry of the uranium dioxide with respect to oxygen content may well be a critical factor associated with the observed diffusion. The stoichiometry of the molybdenum-coated spherical uranium dioxide used in this work will be determined by wet chemical analysis in the near future.

The second factor is that stainless steel, in small amounts, is known to be introduced into the molybdenum used to coat the spherical uranium dioxide during our "in house" proprietary coating process. The exact or average amount of stainless steel pick up is not known, but will be spectrographically determined shortly.

C. Vacuum Emission Test Pellet

Based on the results of the microscopic examination of the sectioned vacuum emission test pellet, described in the previously quarterly report, additional analysis appeared warranted in order to further determine, if possible, the oxygen content of

the uranium dioxide or uranium complex present in the observed inclusions Therefore representative portions of the metallographically sectioned vacuum emission pellet containing inclusions were cut from the initial mount and sent to Advanced Metals Research Corporation for analysis by electron beam microanalysis. In addition, a sample of sintered uranium dioxide of known stoichiometry was included in the mount for use as a standard

The elements present in the grain boundary inclusions were determined by proper positioning of the electron beam Uranium, aluminum, and iron were found to be present. Within the inclusions themselves the presence of aluminum was accompanied by the absence of uranium and, conversely, the presence of uranium was accompanied by the absence of aluminum. The aluminum-rich particles or areas of the inclusions were identified as aluminum oxide by virtue of their visible violet fluorescence, and their presence is attributed to the use of high purity alumina as the polishing media in the sample preparation The presence of alumina in the inclusions is probably also a result of pull out of some of the original uranium dioxide in the inclusion during the sectioning and polishing operations.

The iron that was identified was estimated to be present quantitatively at a level ranging from 0.3 to 0.6 weight percent and its occurrence and quantity did not appear to be dependent on the presence or absence of either aluminum or uranium A plausible explanation for the presence of iron in the inclusion is the known iron pickup which occurs during the process used to coat the spherical uranium dioxide with molybdenum. A spectrographic determination of the amount of iron in a typical sample of molybdenum-coated spherical uranium dioxide will be conducted at Martin in the near future

A careful search of the inclusions, using the UM_{β}, UM_{α}, and UM_{γ} spectral emission lines, showed the presence of uranium rich areas which were quite small relative to the size of the entire inclusion The size of these areas precluded the possibility of determining the precise concentration of the uranium or its stoichiometry. The uranium was qualitatively identified as being present as uranium dioxide by

virtue of its faint blue visible fluorescence under excitation by the electron beam. Further analysis appears inadvisable at this time since presently available techniques are not capable of providing a more precise quantitative analysis of the composition of the inclusions.

D. Plans for the Next Quarterly Period

Future plans, with respect to the materials phase of the program, include examination of the fueled emitters from the double module thermionic converter upon completion of performance testing. No additional analysis of the grain boundary inclusions noted in the thermal conductivity test pellets is planned because of their similarity to the inclusions noted in the vacuum emission pellet, and the lack of a sufficiently precise quantitative analysis technique with which to conduct the investigation. Spectrographic analysis of the molybdenum coating on the spherical uranium dioxide will be run on several lots of material to determine characteristic iron content levels, and the stoichiometry of the molybdenum-coated uranium dioxide will be determined by wet chemical analysis.

IV. Advanced Module Design

Work to generate the engineering design of an advanced double diode converter was initiated during this quarterly period.

A. Advanced Module Design Philosophy

The converter design to be generated will reflect, where appropriate, the incorporation of new materials, component designs, and general arrangements which, based on the results of prior and current efforts (double diode converter work including the FDM-1 and its Martin-sponsored predecessors, Martin-sponsored single diode converter efforts, fuel form and fuel pellet development activities, and the fuel pellet vacuum emission experiment) appear desirable to obtain improved performance and simple installation and operation. The advanced converter will be designed for laboratory-type testing and be similar in configuration to the FDM-1. However, it will be oriented as much as possible toward the presently anticipated requirements for a future in-pile test. Consideration will be given to modifications which will ultimately permit electrically heated operation and check-out followed by in-pile testing of the same device. This dual operational approach is highly desirable since it improves the level of confidence in a particular device especially during the initial phases of a development program.

B. Accomplishments

A critical review and evaluation of the FDM-1 converter design has been performed in the light of test results obtained to date. Some preliminary modifications to the FDM-1 device which will be incorporated into the advanced converter design have been established and include:

a. Both collectors will be sprayed with an insulating coating to duplicate the electrical and thermal characteristics appropriate to a multi-diode fuel element as opposed to the present design in which only one anode is sprayed and the other forms an integral part of the casing.

b. The arrangement of the exterior components used for waste heat removal will be modified to permit a more compact design compatible with the geometric requirements of an in-pile test device.

C. Plans for the Next Quarterly Period

During the next quarterly period, development of the advanced module design will be completed. Drawings presenting the detailed design of the advanced double diode converter and associated test fixtures will be prepared. The drawings will be sufficiently detailed to the point that fabrication could be initiated in the future.

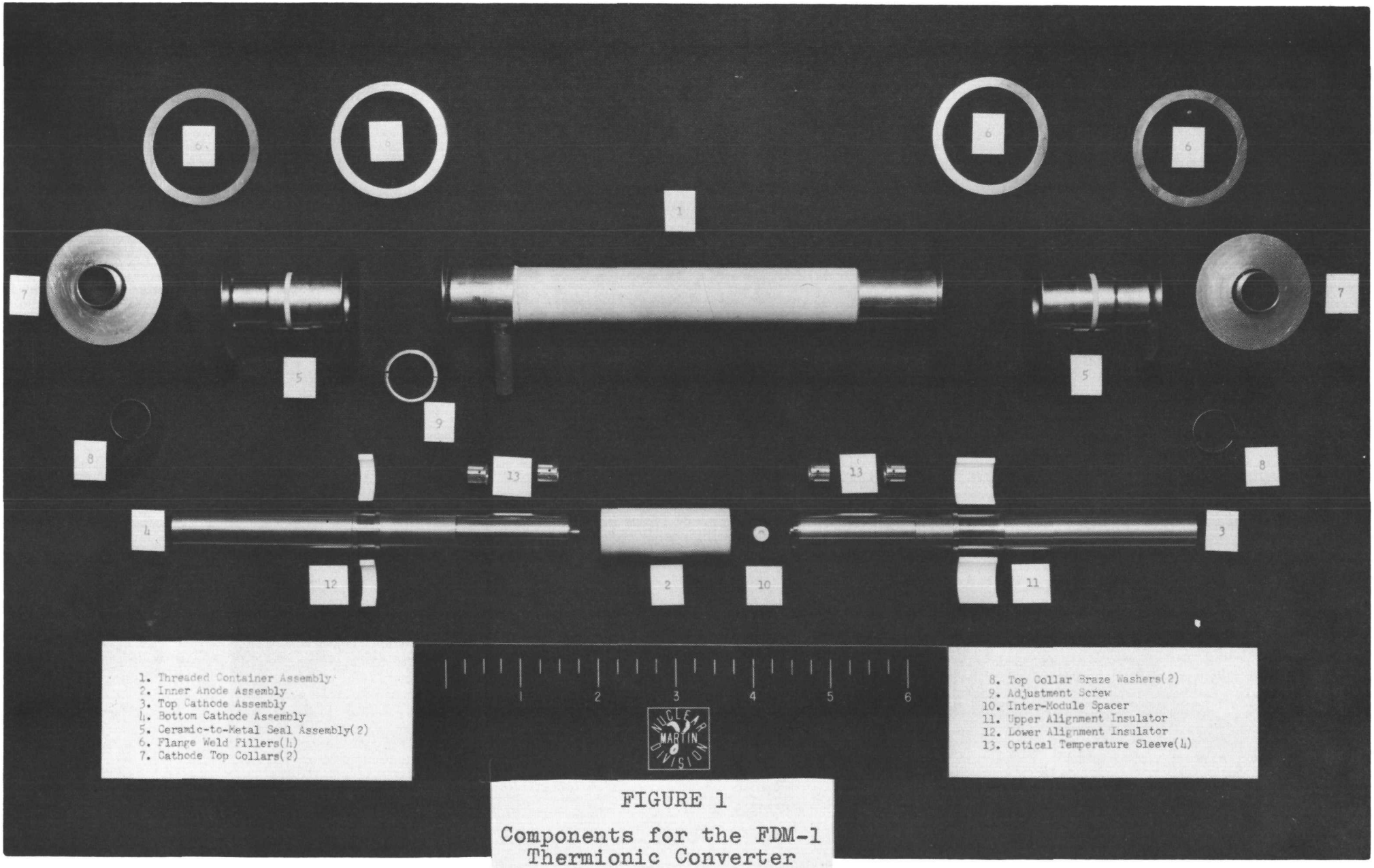

FIGURE 1

Components for the FDM-1
Thermionic Converter

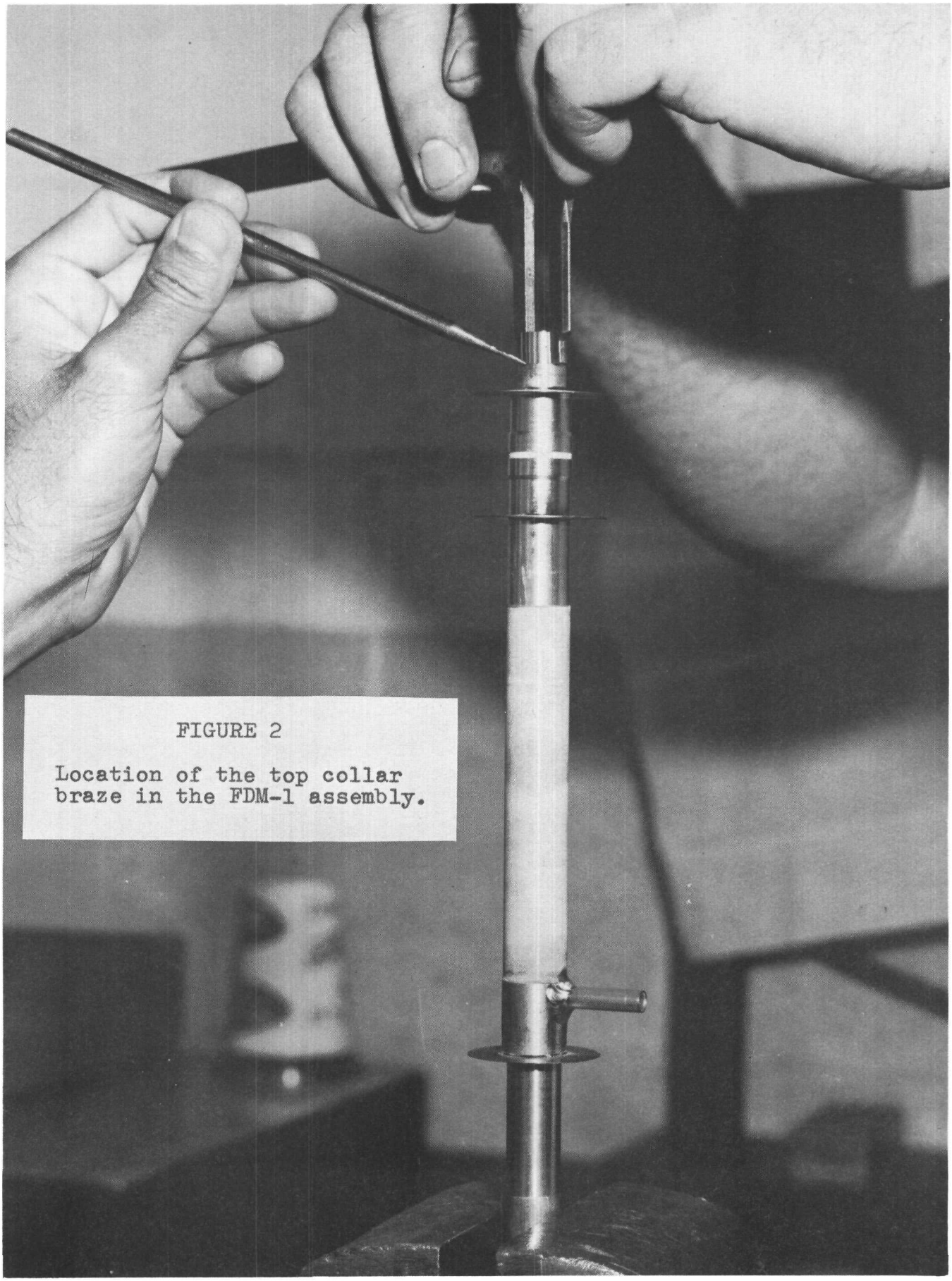

FIGURE 2

Location of the top collar braze in the FDM-1 assembly.

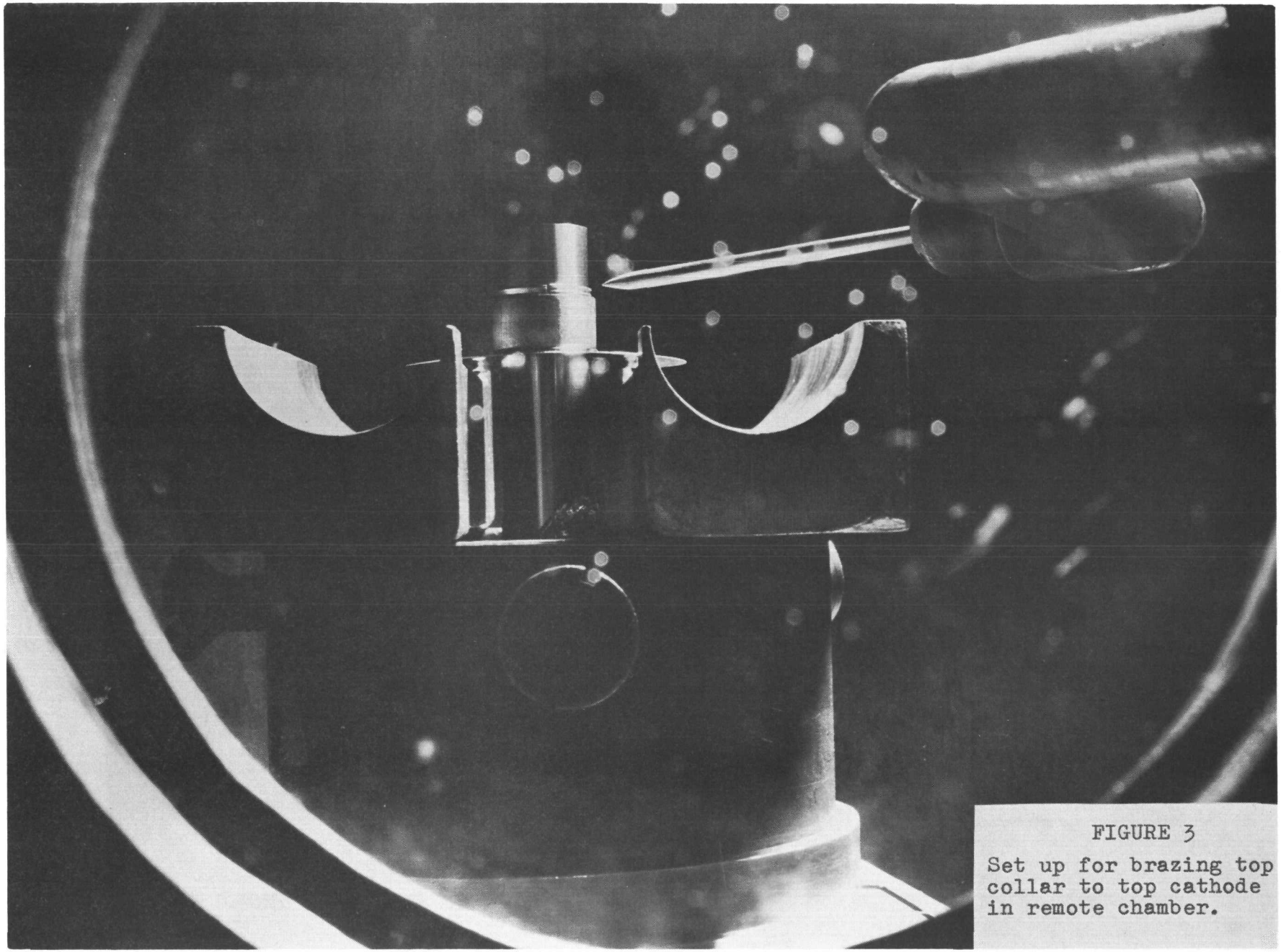

FIGURE 3

Set up for brazing top collar to top cathode in remote chamber.

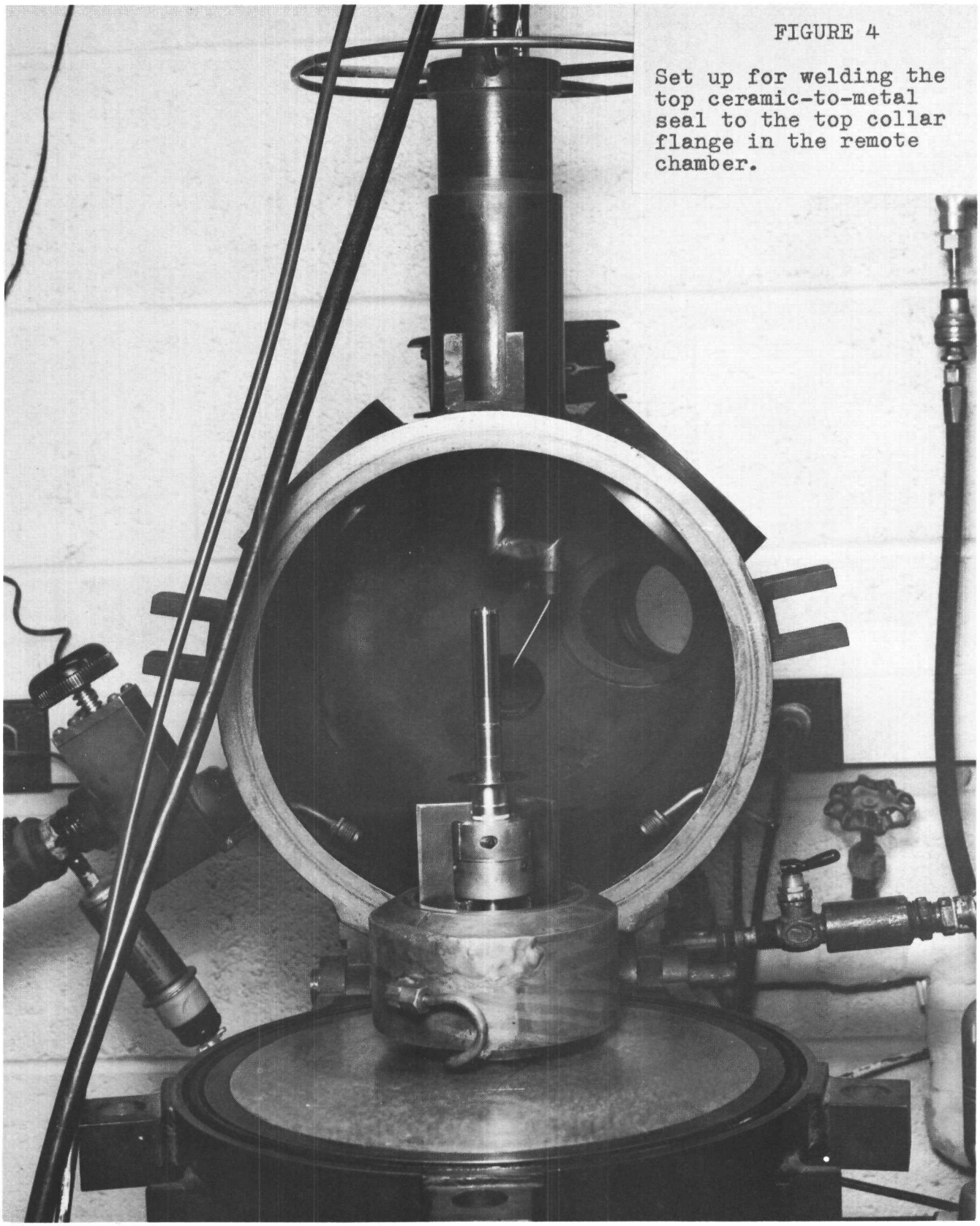

FIGURE 4

Set up for welding the top ceramic-to-metal seal to the top collar flange in the remote chamber.

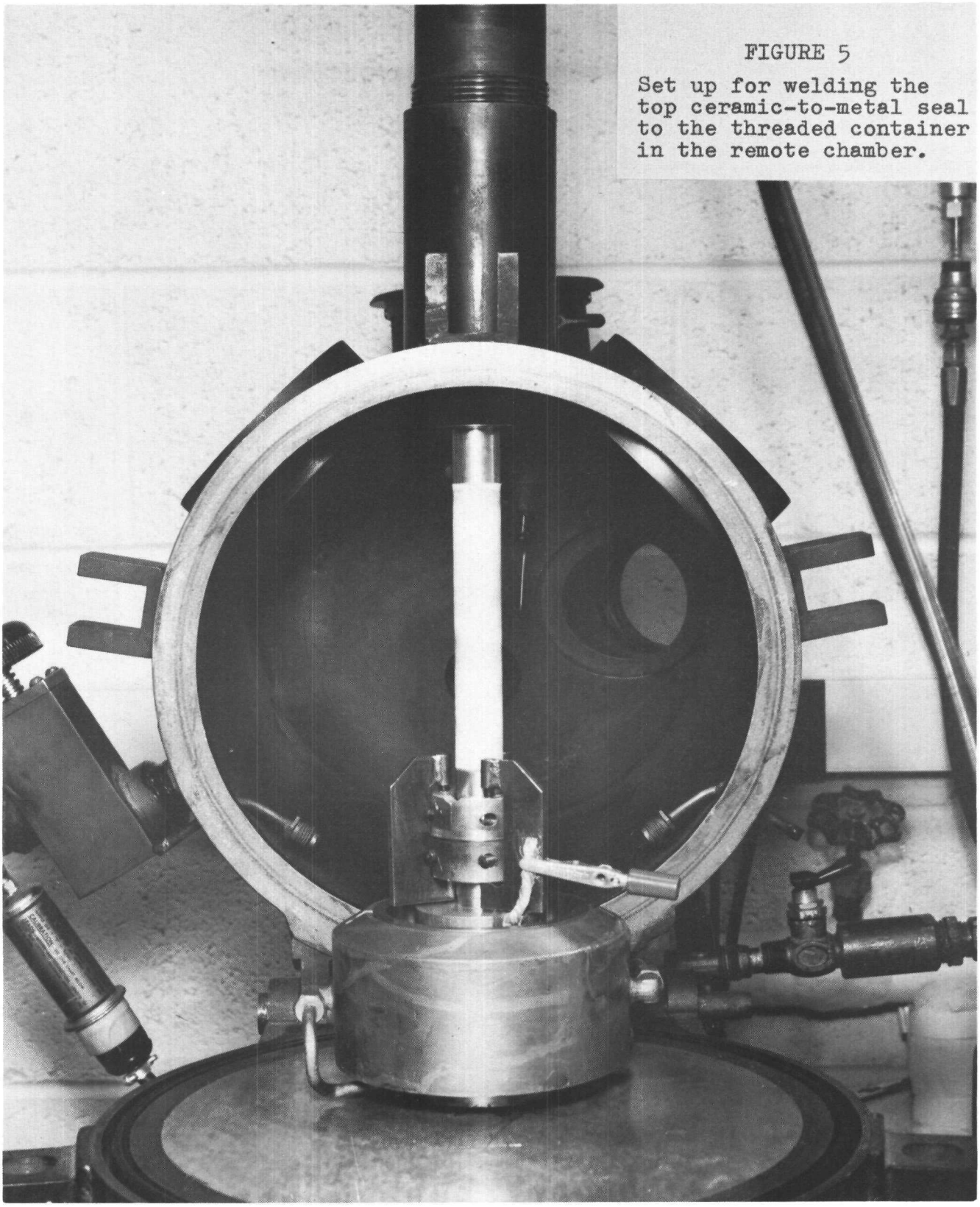

FIGURE 5

Set up for welding the top ceramic-to-metal seal to the threaded container in the remote chamber.

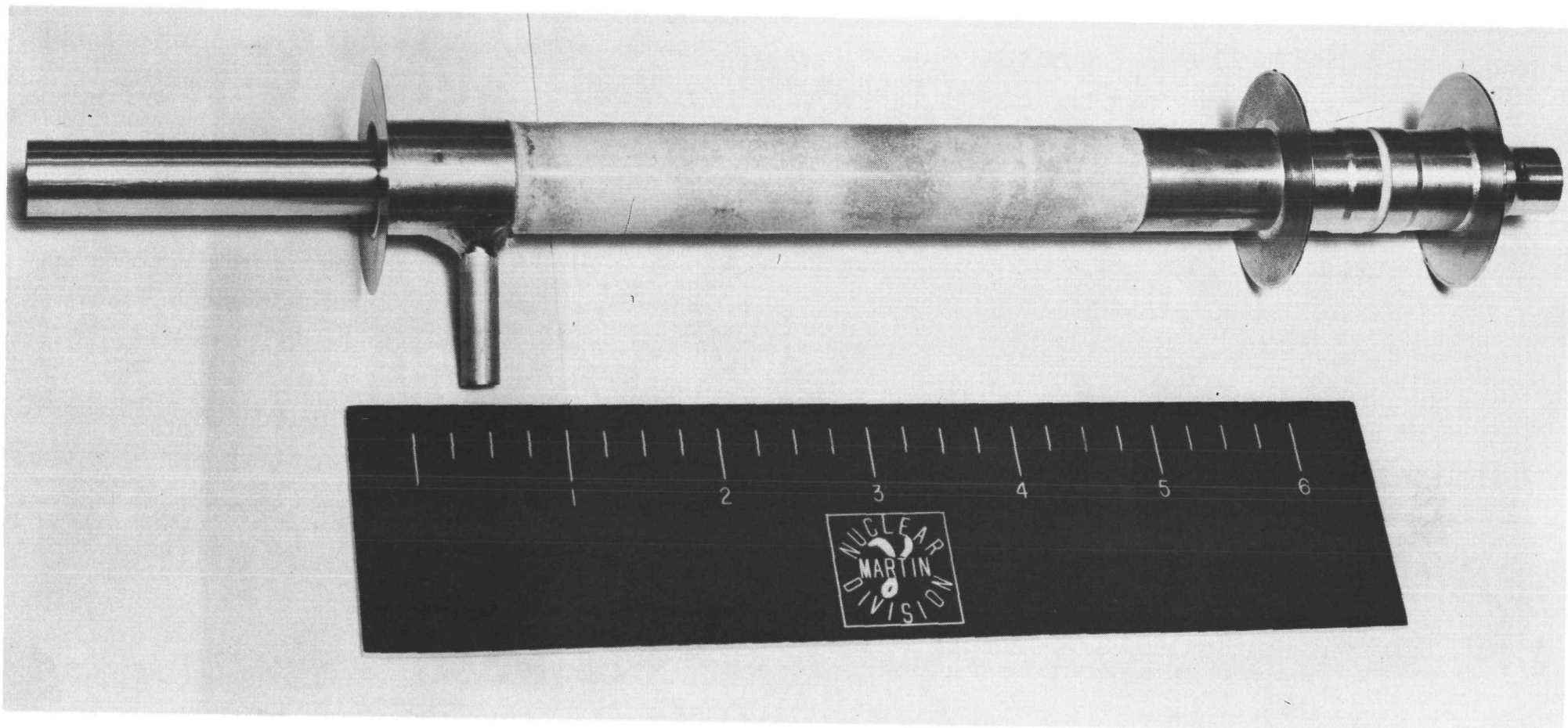

FIGURE 6

FDM-1 assembly with bottom cathode located prior to gammagraph and subsequent assembly.

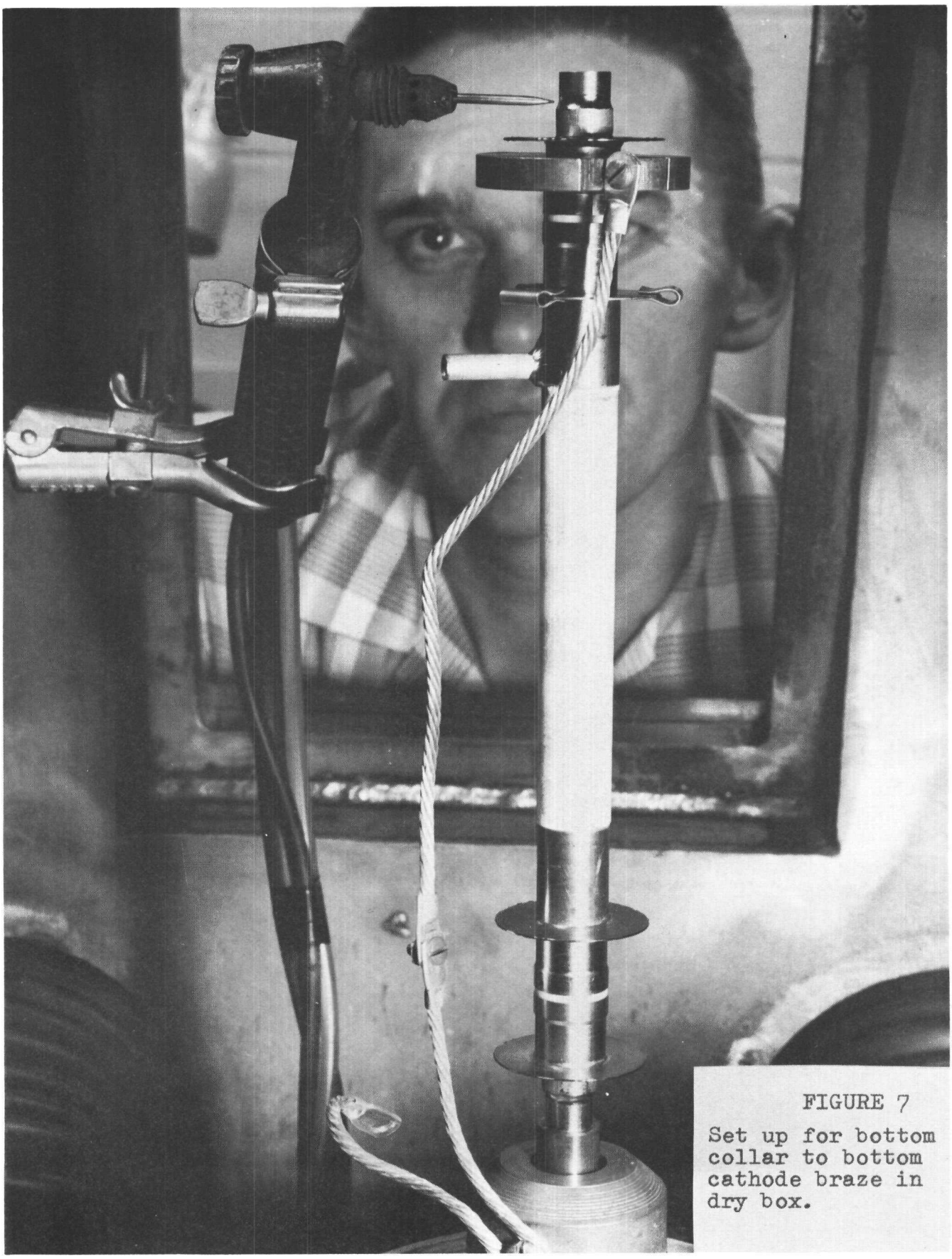

FIGURE 7

Set up for bottom collar to bottom cathode braze in dry box.

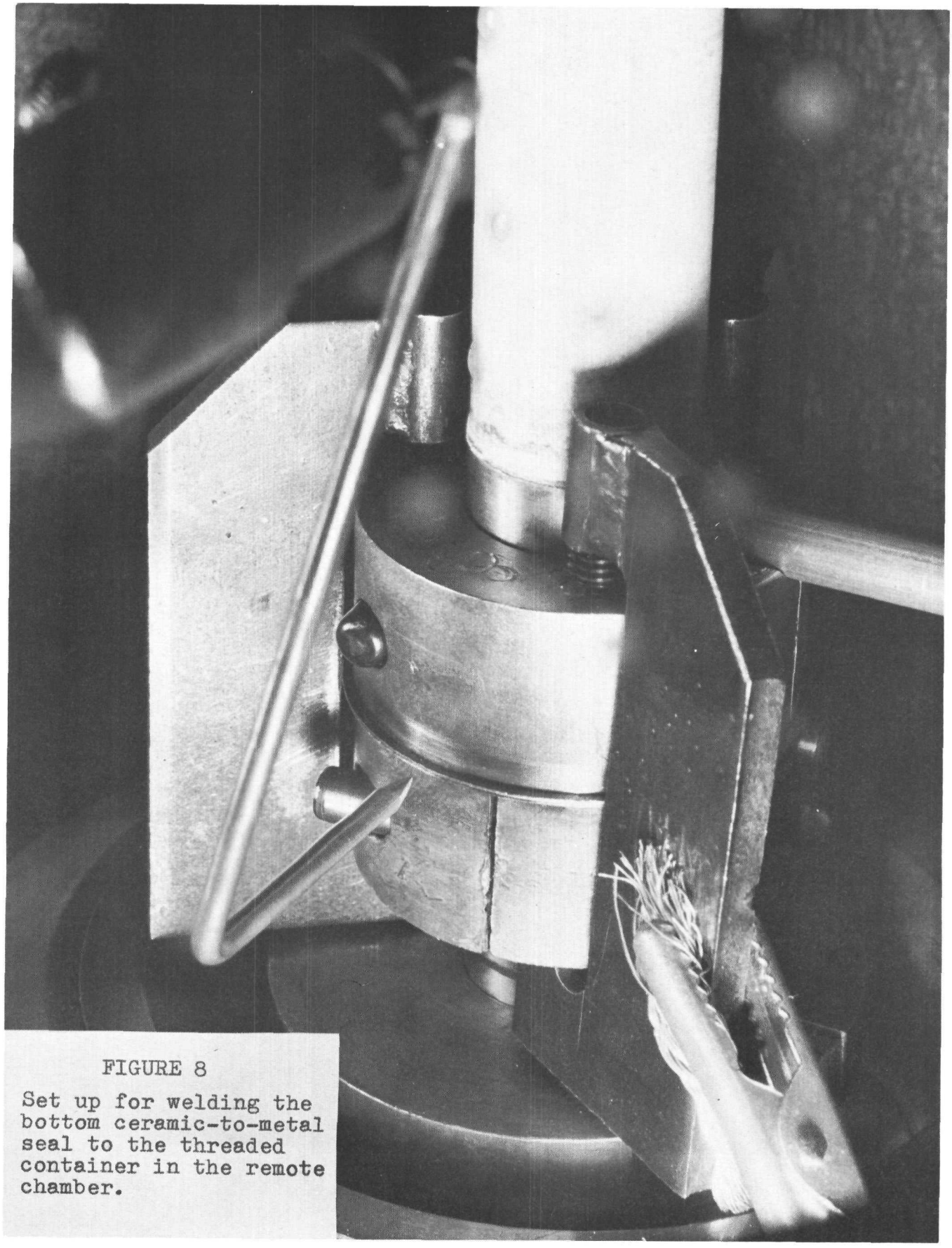

FIGURE 8

Set up for welding the bottom ceramic-to-metal seal to the threaded container in the remote chamber.

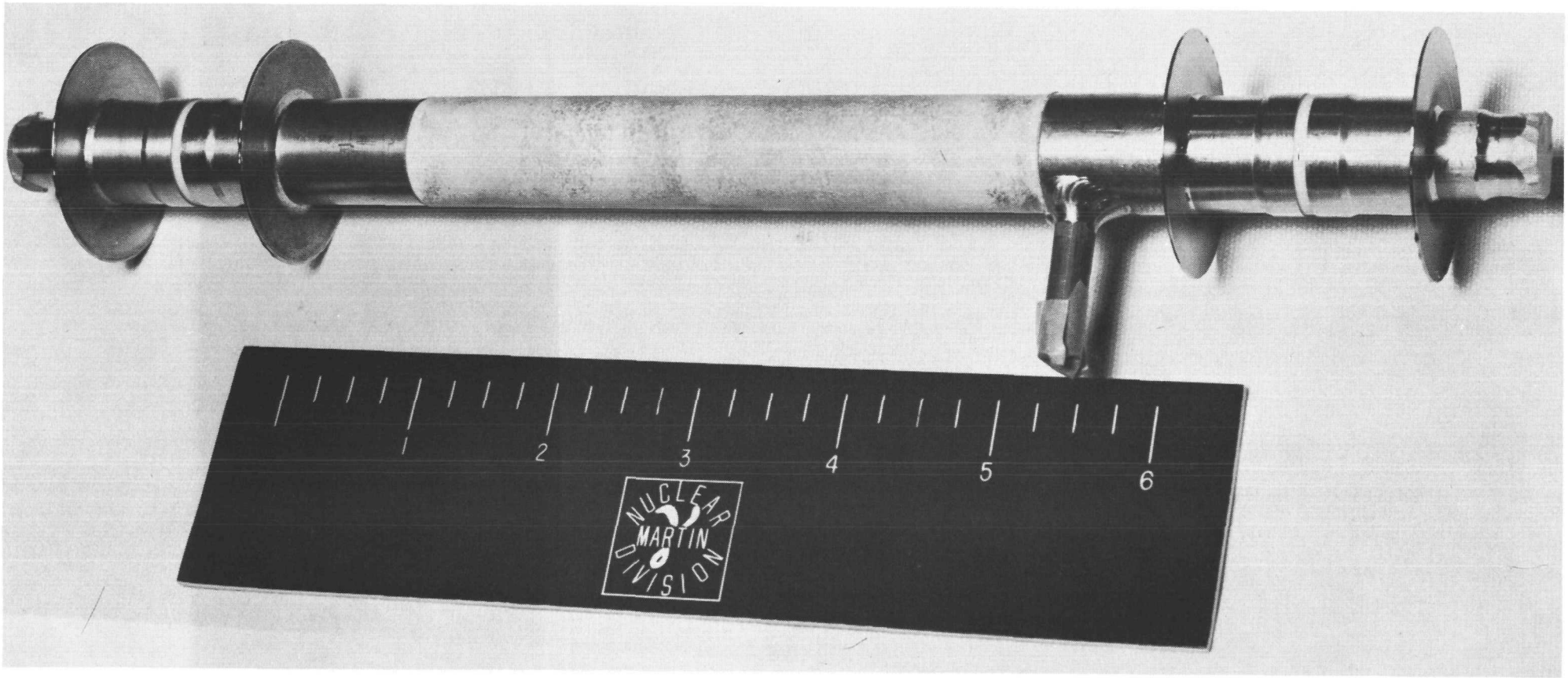

FIGURE 9

View of basic FDM-1 converter assembly with leak testing and gammagraphing complete.

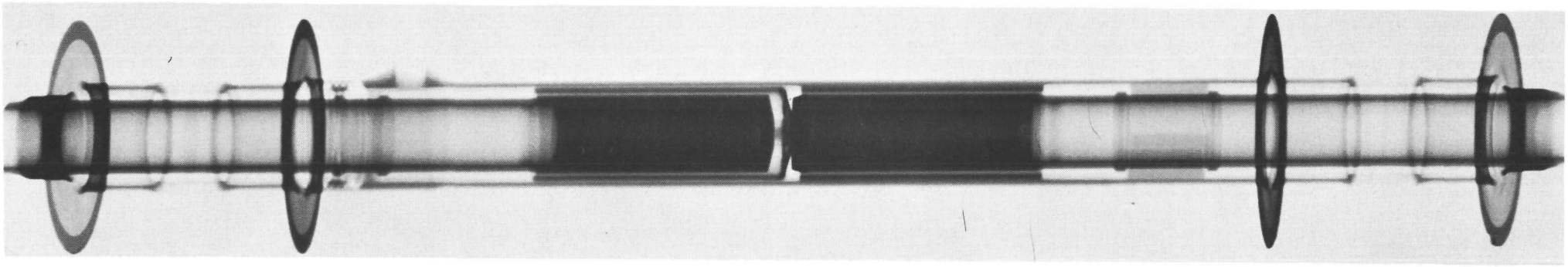

FIGURE 10. Gammagraph print of the FDM-1 converter assembly.

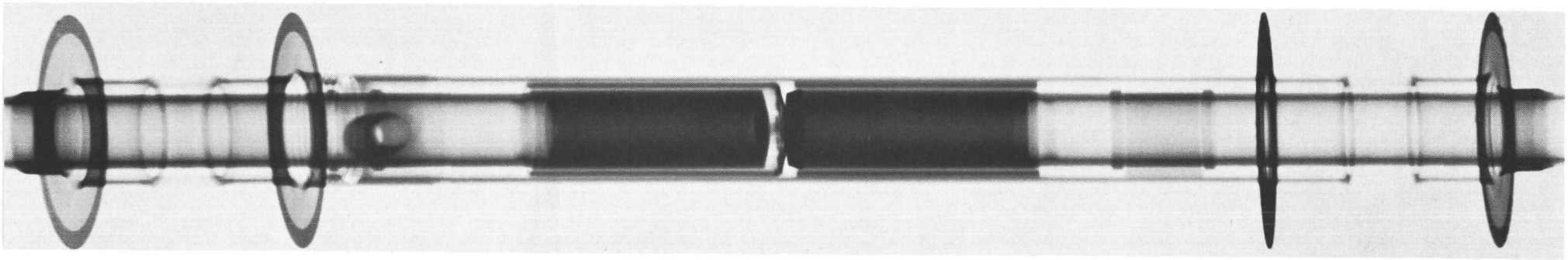

FIGURE 11. View taken 120° from that of Figure 10.

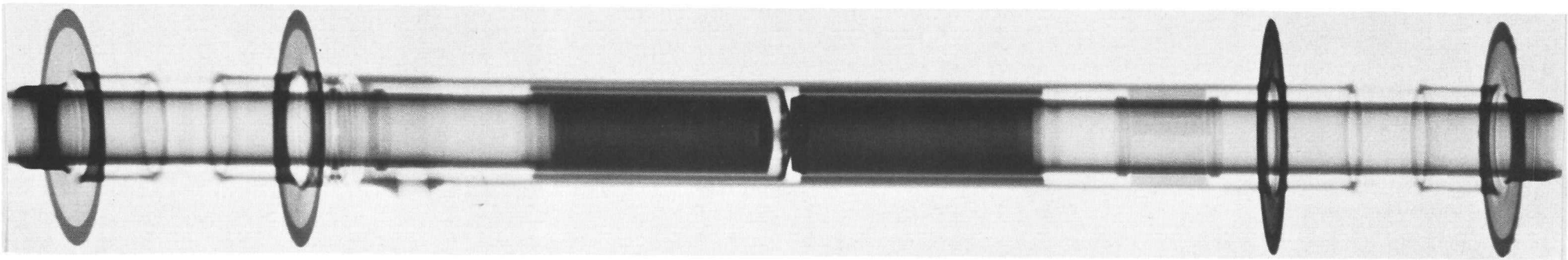

FIGURE 12. View taken 120° from that of Figure 11.

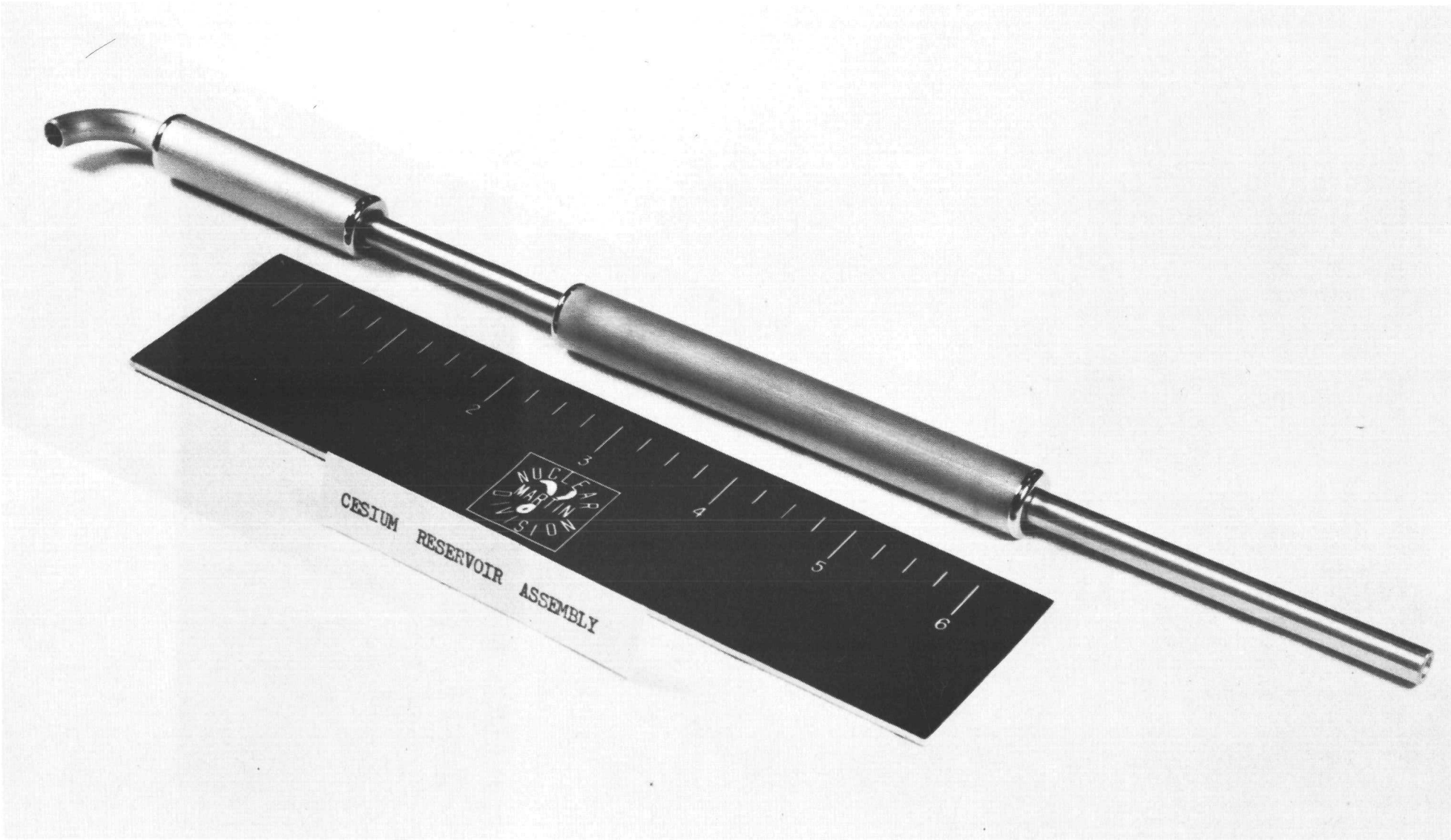

FIGURE 13

Cesium reservoir assembly for the FDM-1 converter.

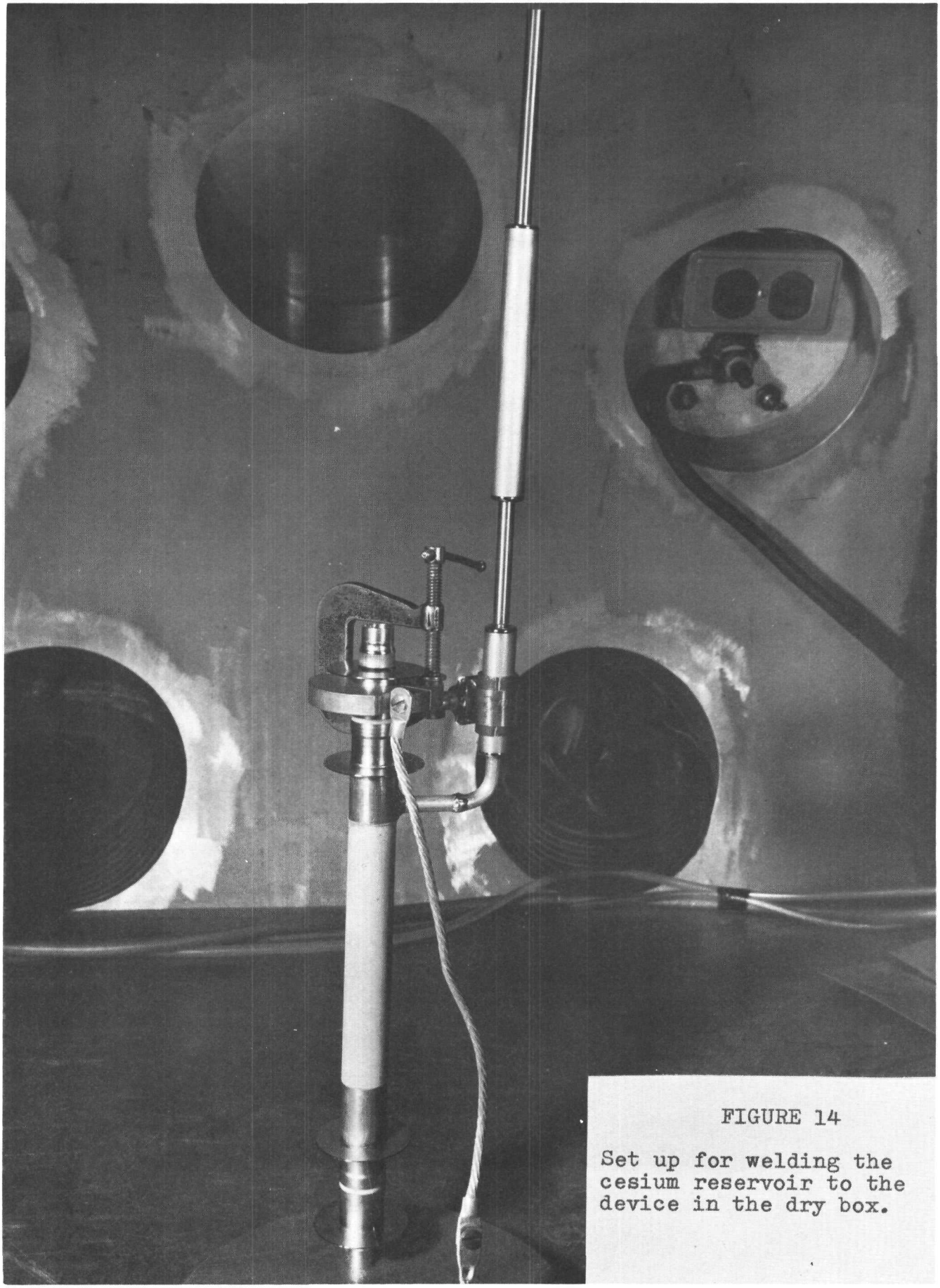

FIGURE 14

Set up for welding the cesium reservoir to the device in the dry box.

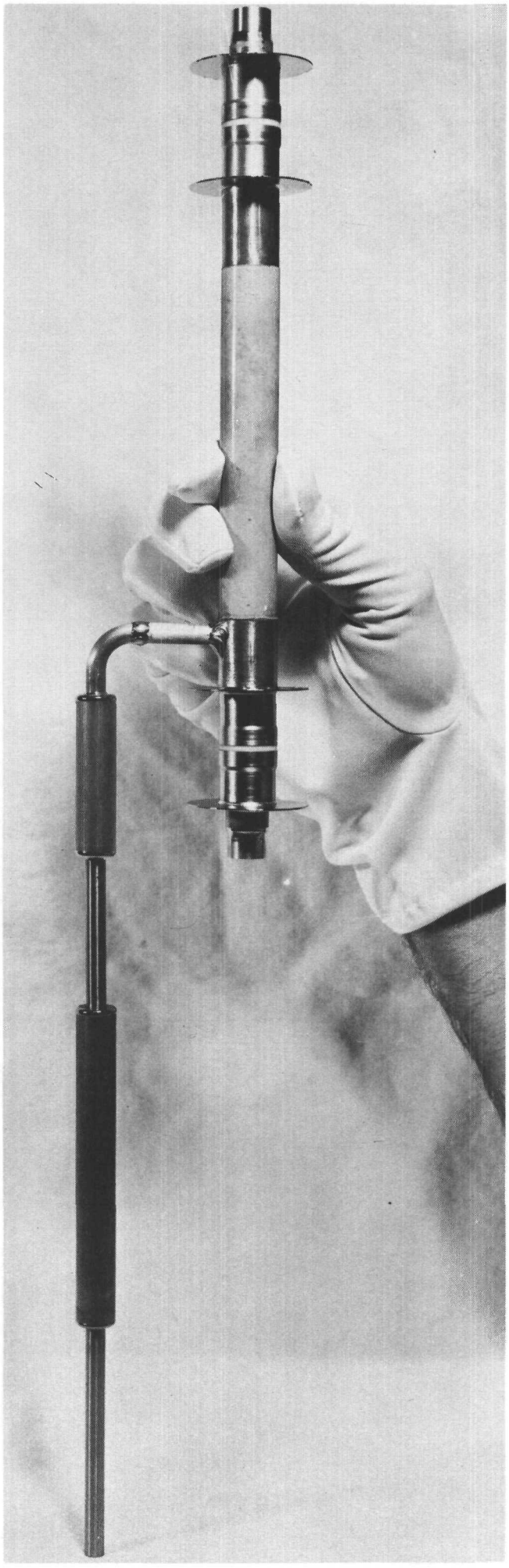

FIGURE 15

Completed FDM-1 converter assembly.

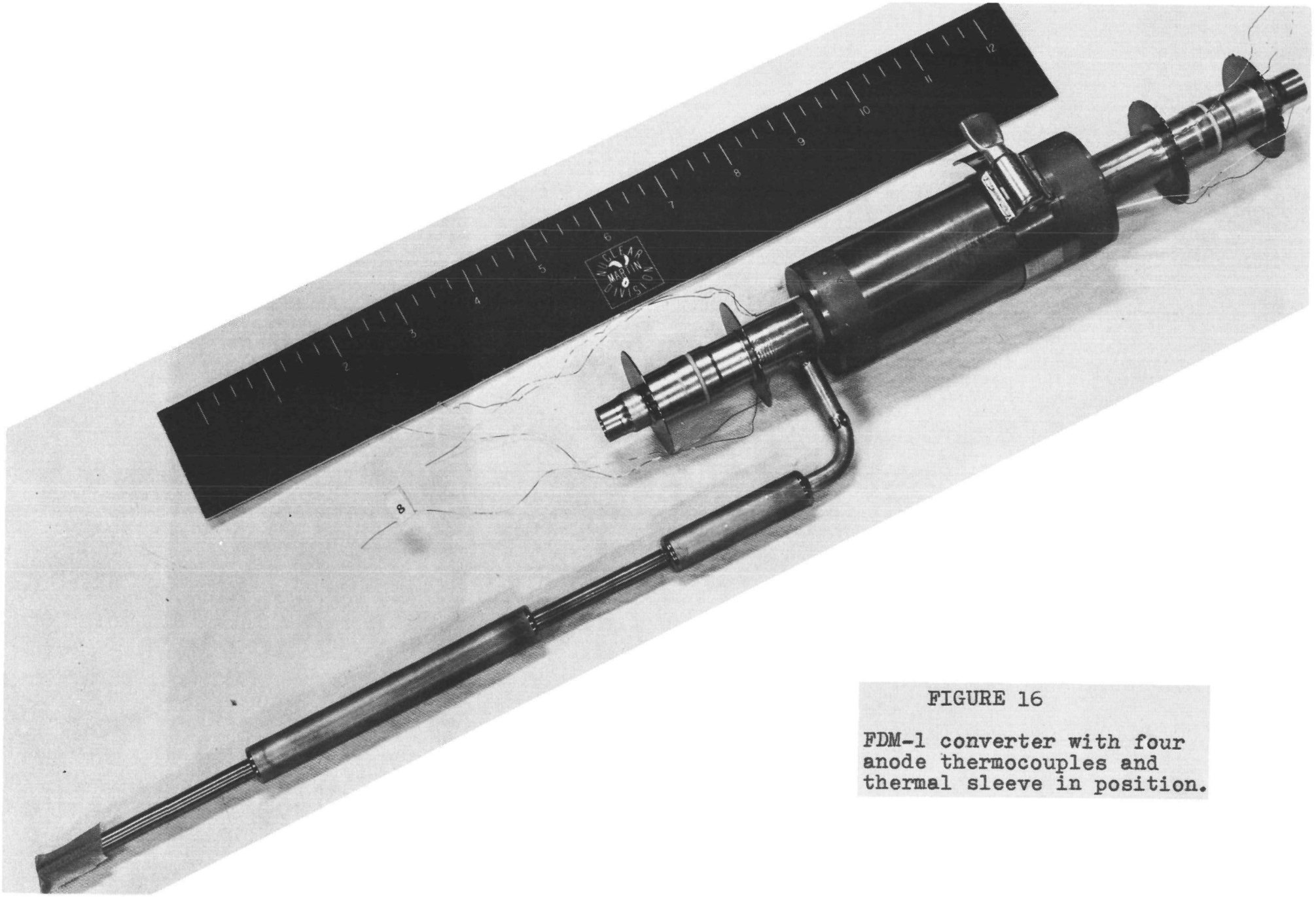

FIGURE 16

FDM-1 converter with four anode thermocouples and thermal sleeve in position.

FIGURE 17

Positioning an optical temperature viewing sleeve for insertion into the FDM-1 assembly.

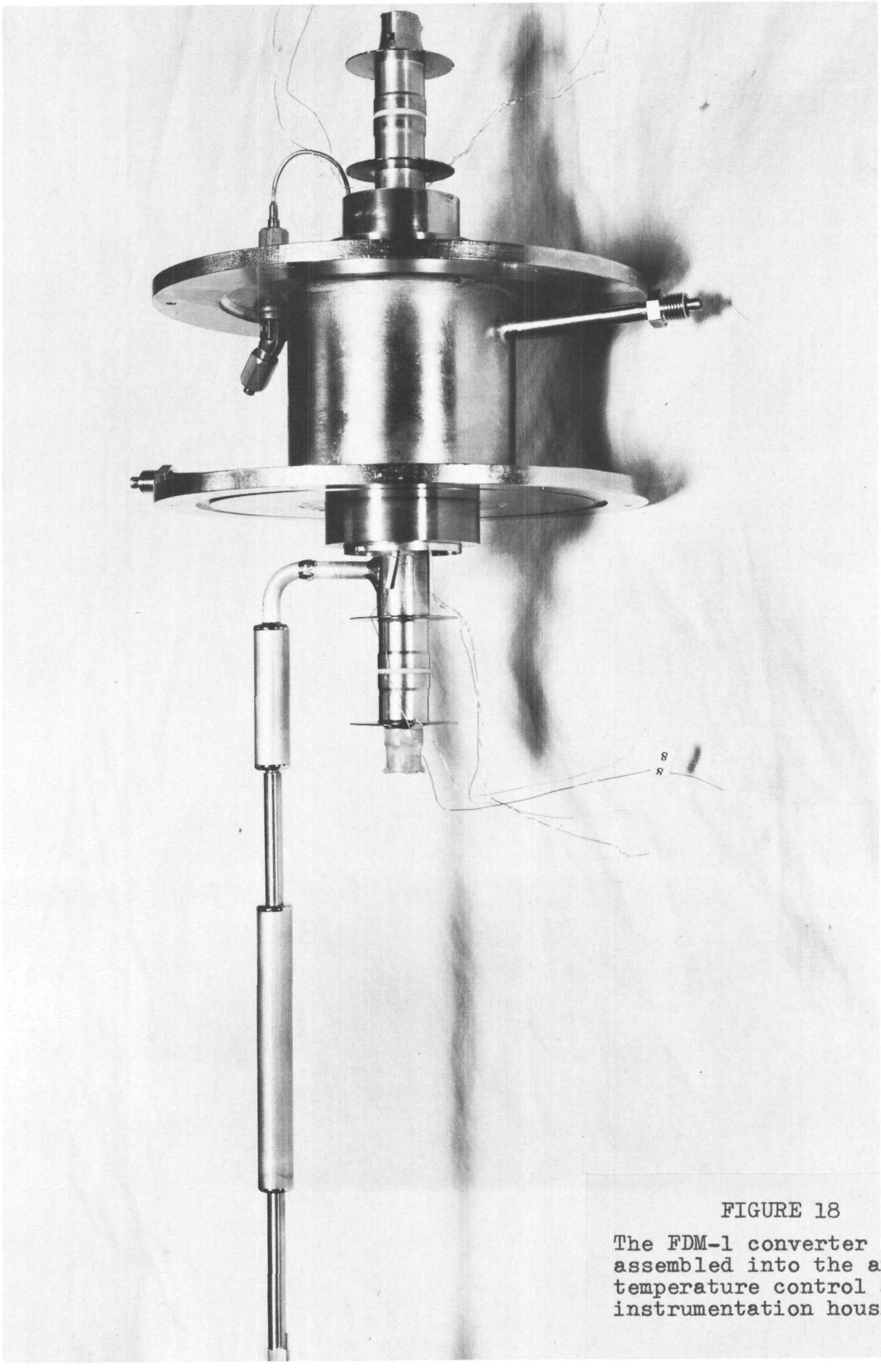

FIGURE 18

The FDM-1 converter assembled into the anode temperature control and instrumentation housing.

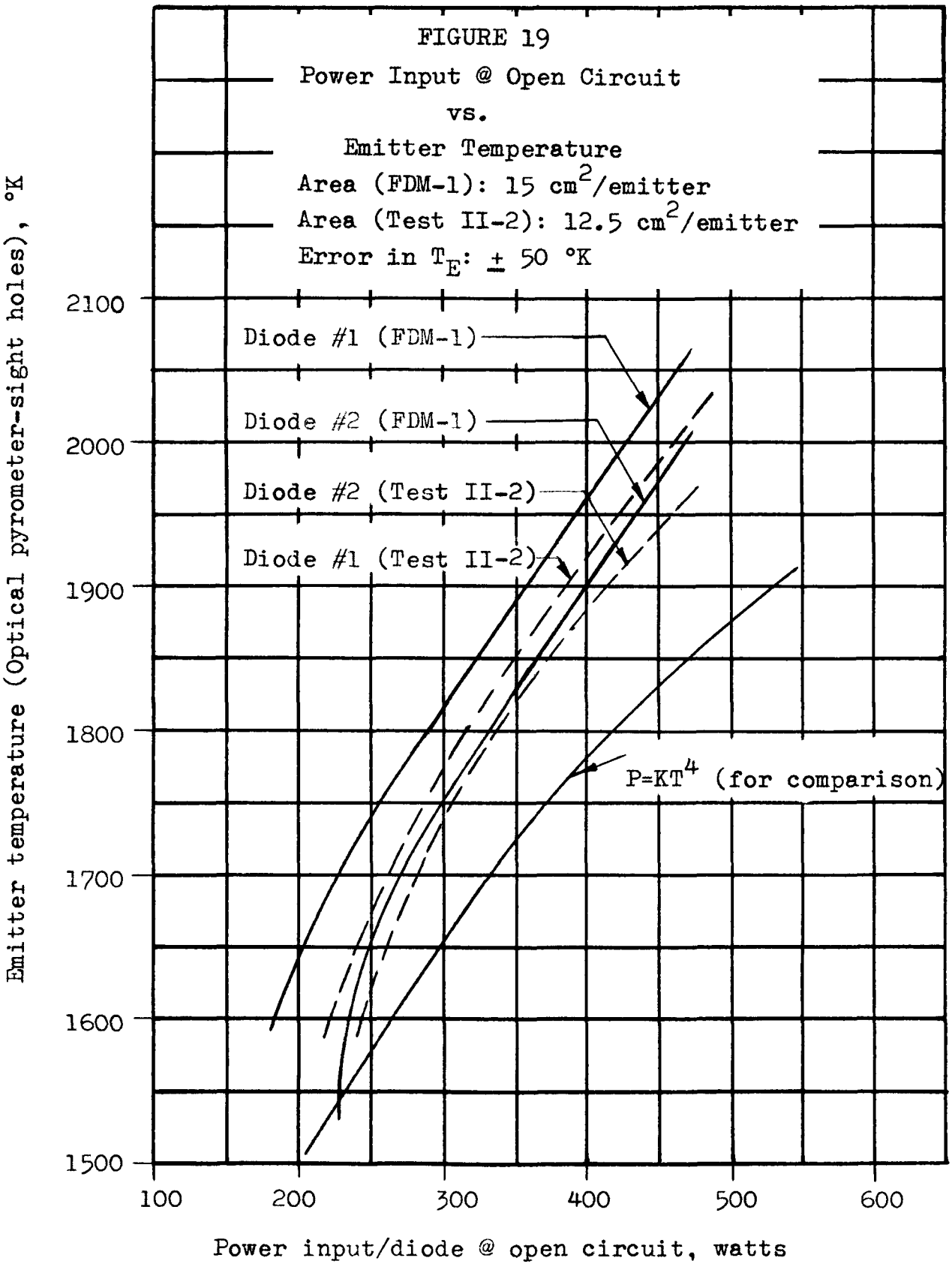
FIGURE 19
Power Input @ Open Circuit
vs.
Emitter Temperature
Area (FDM-1): 15 cm^2/emitter
Area (Test II-2): 12.5 cm^2/emitter
Error in T_E: ± 50 °K
Diode #1 (FDM-1)
Diode #2 (FDM-1)
Diode #2 (Test II-2)
Diode #1 (Test II-2)
$P=KT^4$ (for comparison)
Emitter temperature (Optical pyrometer-sight holes), °K
2100
2000
1900
1800
1700
1600
1500
100
200
300
400
500
600
Power input/diode @ open circuit, watts

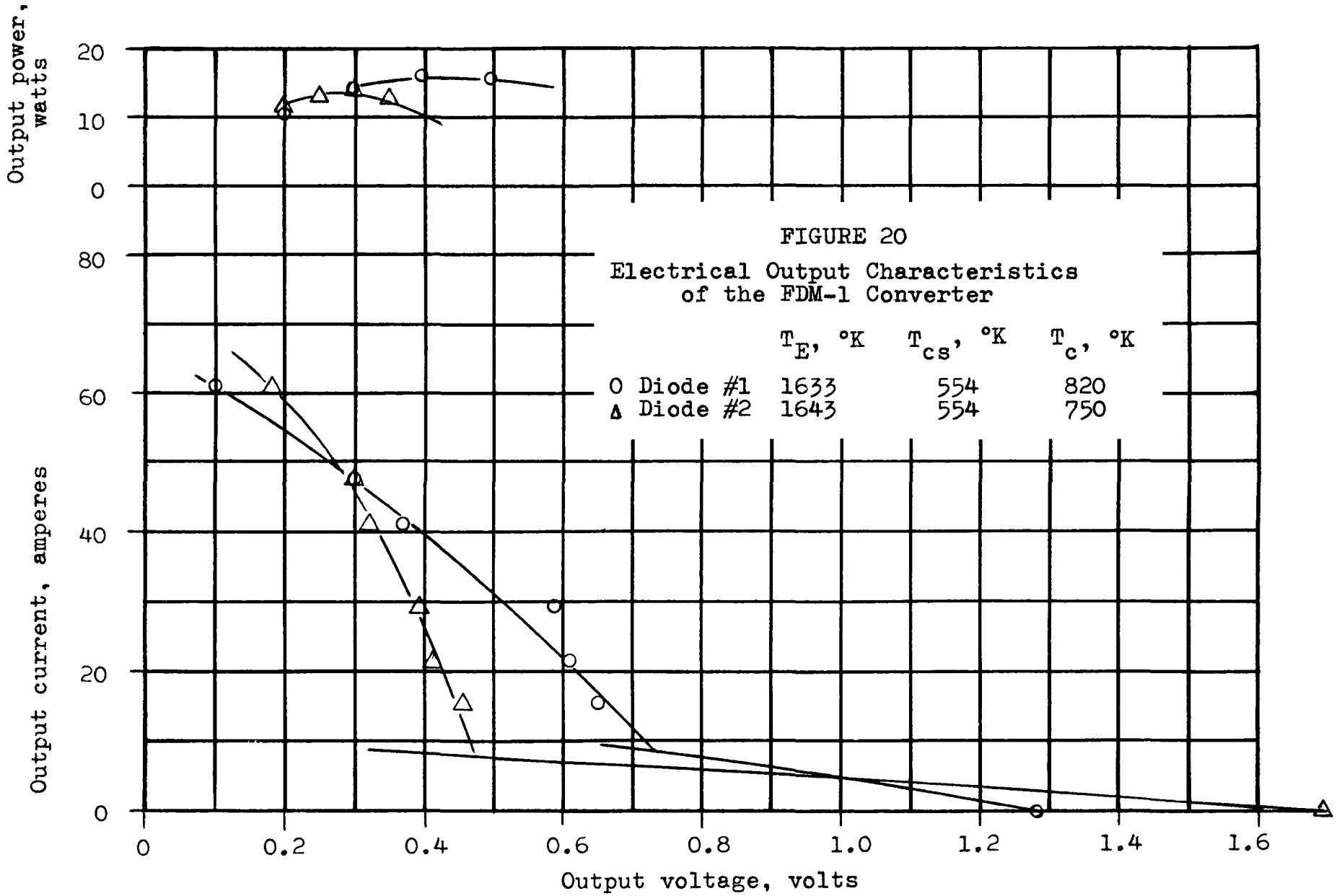

FIGURE 20

Electrical Output Characteristics of the FDM-1 Converter

	T_E, °K	T_{cs}, °K	T_c, °K
O Diode #1	1633	554	820
Δ Diode #2	1643	554	750

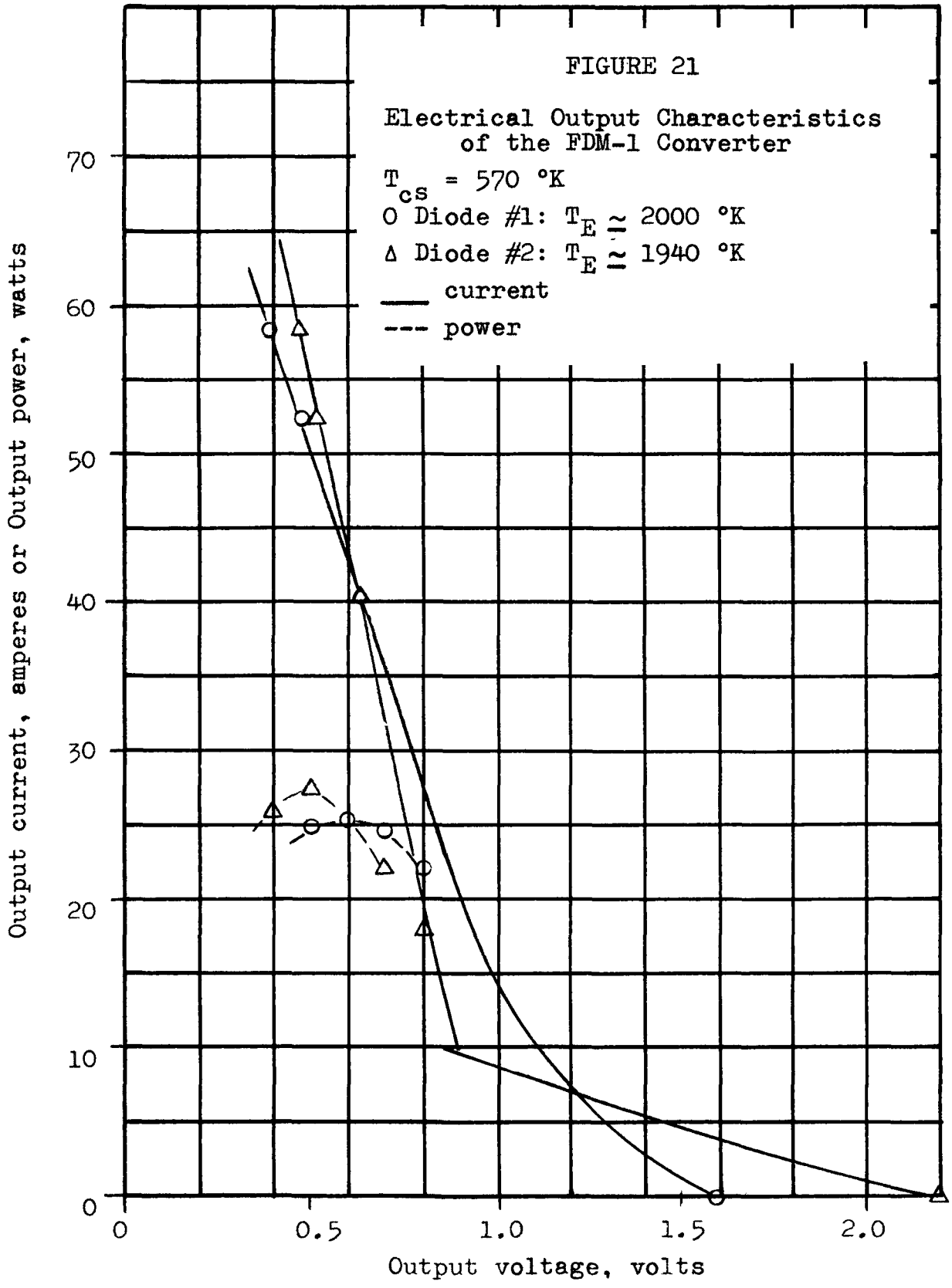
FIGURE 21
Electrical Output Characteristics of the FDM-1 Converter
T_{cs} = 570 °K
O Diode #1: $T_E \simeq$ 2000 °K
Δ Diode #2: $T_E \simeq$ 1940 °K
current
power
Output current, amperes or Output power, watts
0
10
20
30
40
50
60
70
0
0.5
1.0
1.5
2.0
Output voltage, volts

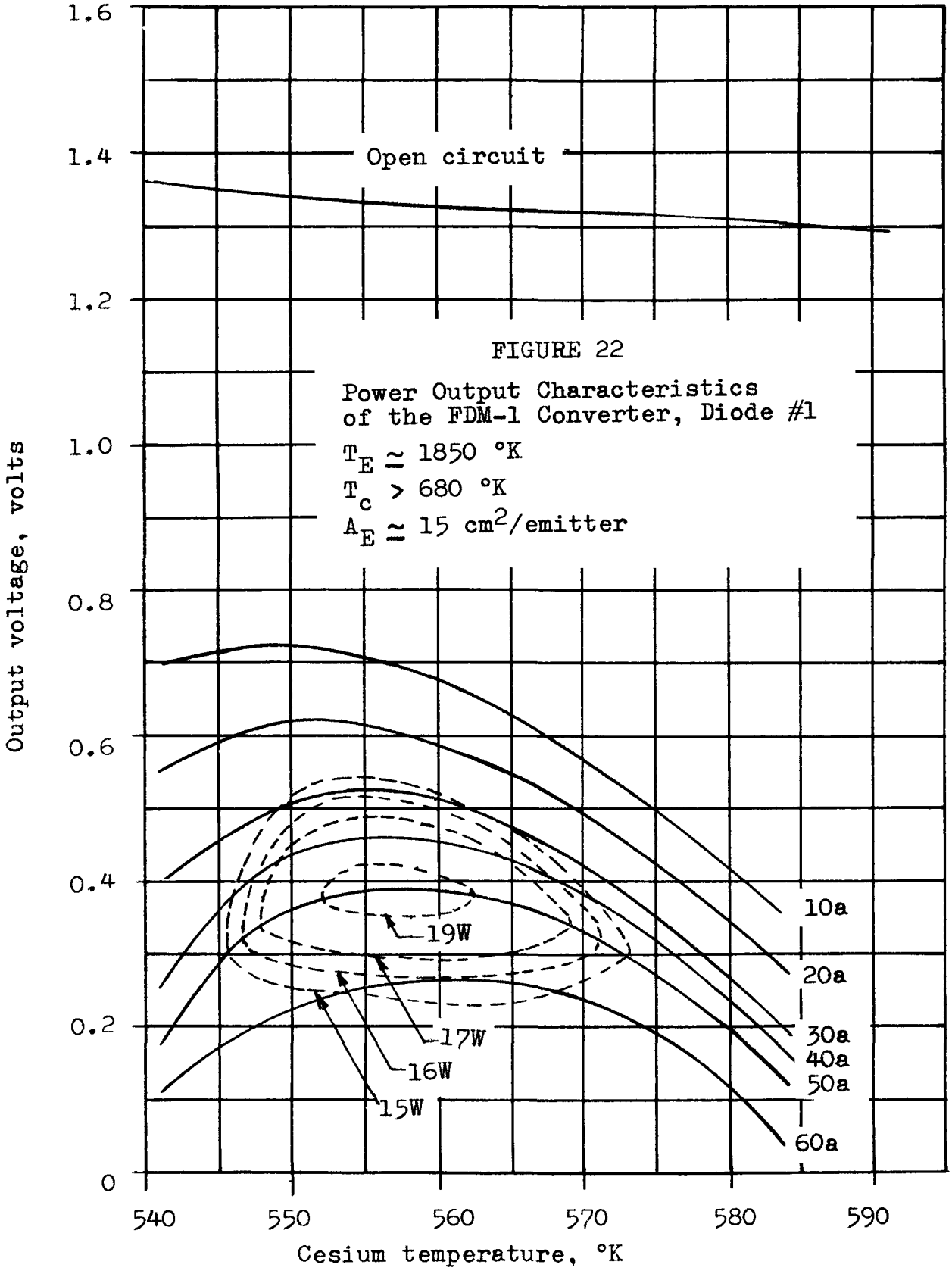

FIGURE 22

Power Output Characteristics
of the FDM-1 Converter, Diode #1

$T_E \simeq 1850$ °K

$T_c > 680$ °K

$A_E \simeq 15$ cm^2/emitter

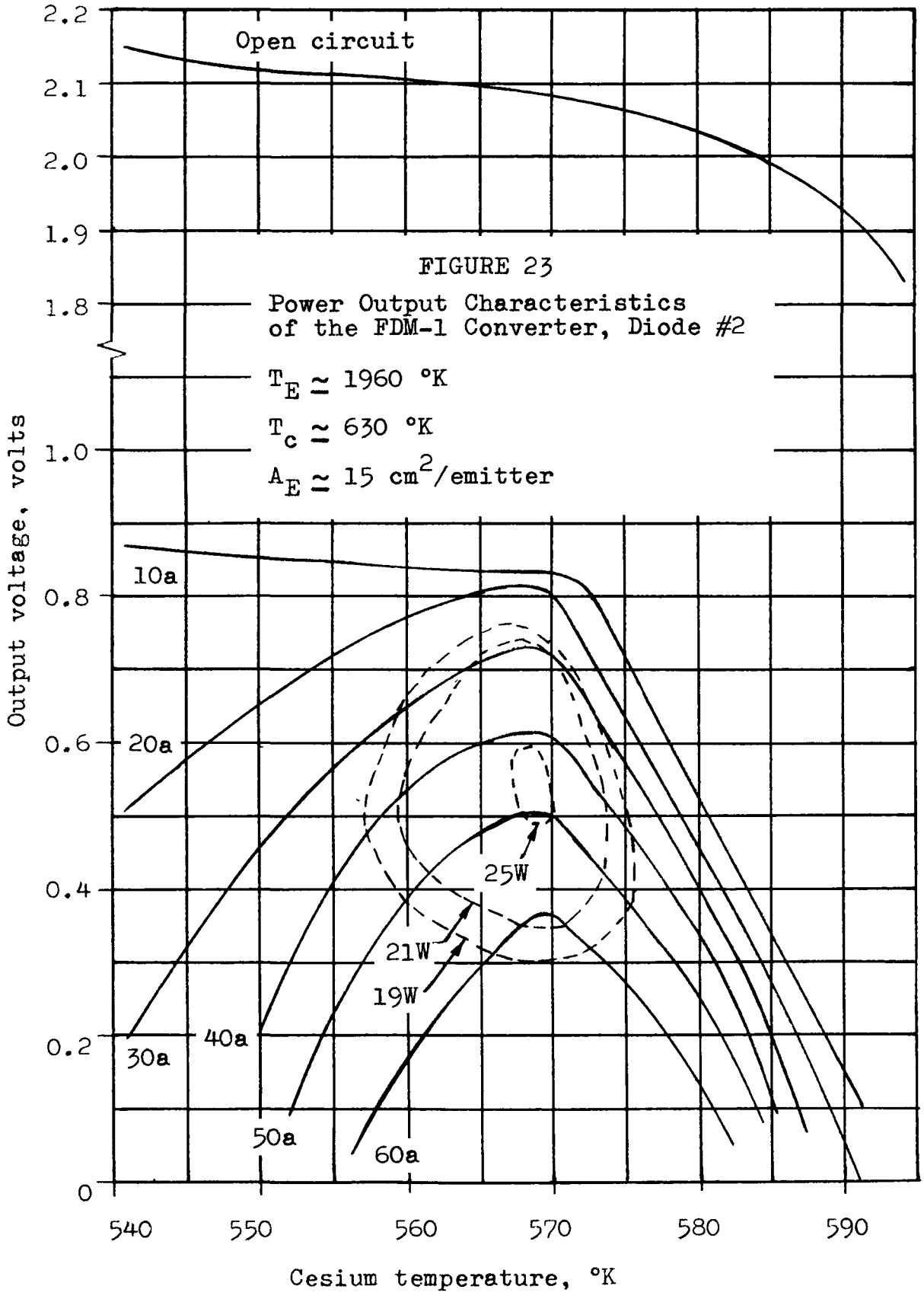

FIGURE 23

Power Output Characteristics of the FDM-1 Converter, Diode #2

$T_E \simeq 1960$ °K

$T_c \simeq 630$ °K

$A_E \simeq 15$ cm^2/emitter

FIGURE 24
Operational History of the FDM-1 Converter
Lifetime Temperature Profile

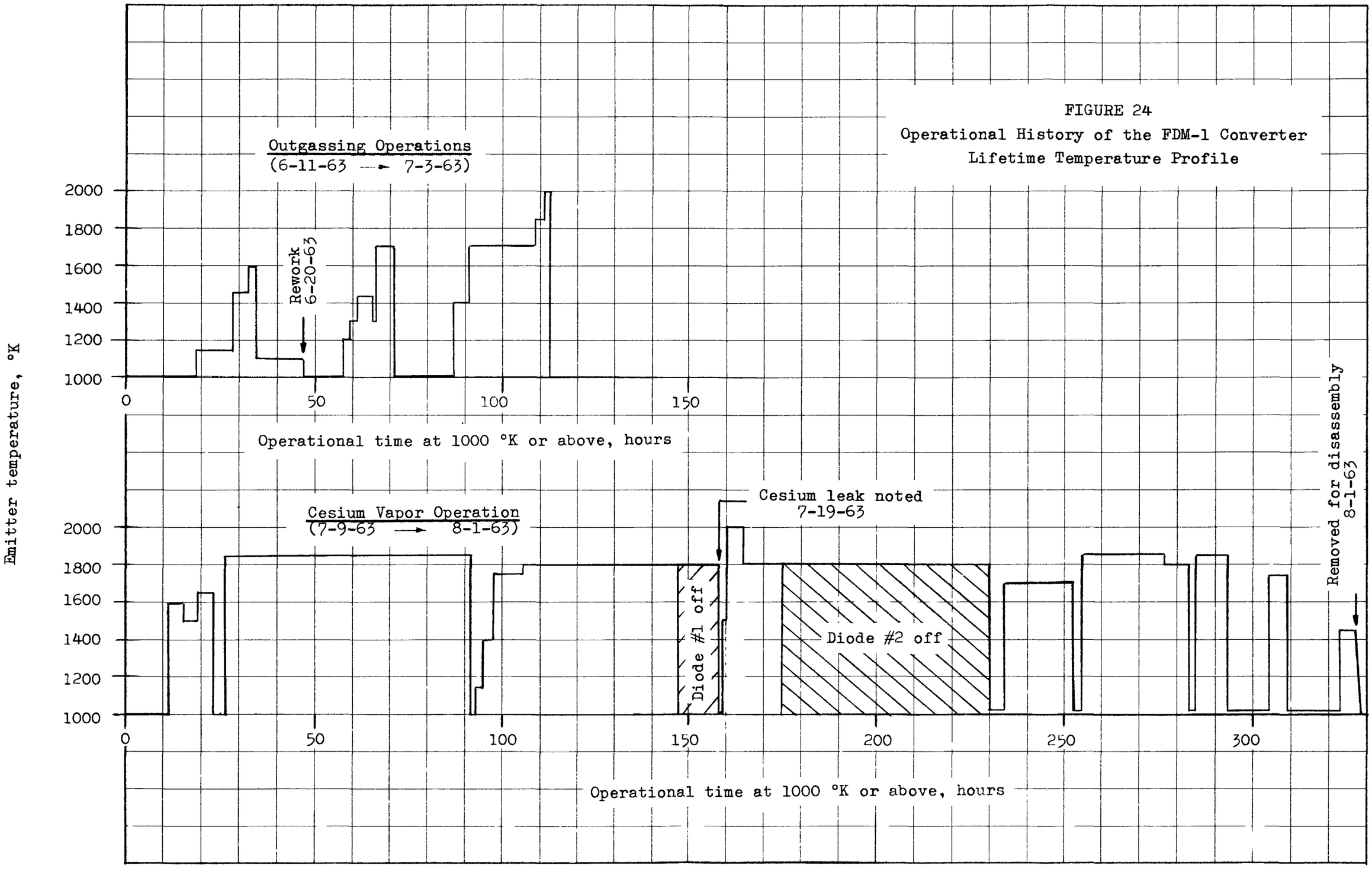

FIGURE 25

Thermal Conductivity of the UO_2-Mo System Before & After 500 Hour Thermal Endurance Test at 1550°C

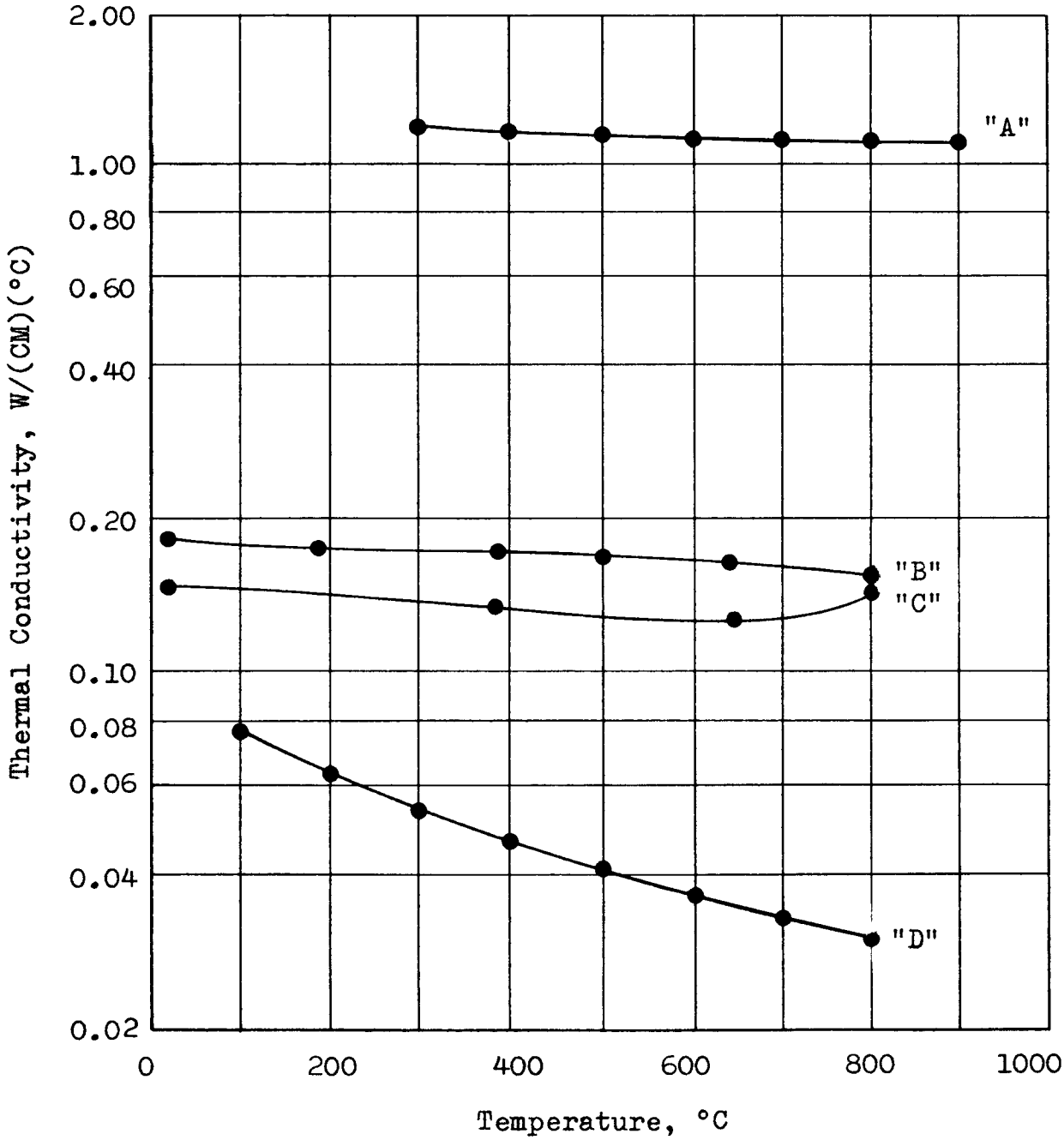

Legend

Curve "A" - Molybdenum
Curve "B" - UO_2-Mo; After Thermal Endurance Test
Curve "C" - UO_2-Mo; Before Thermal Endurance Test
Curve "D" - Sintered UO_2

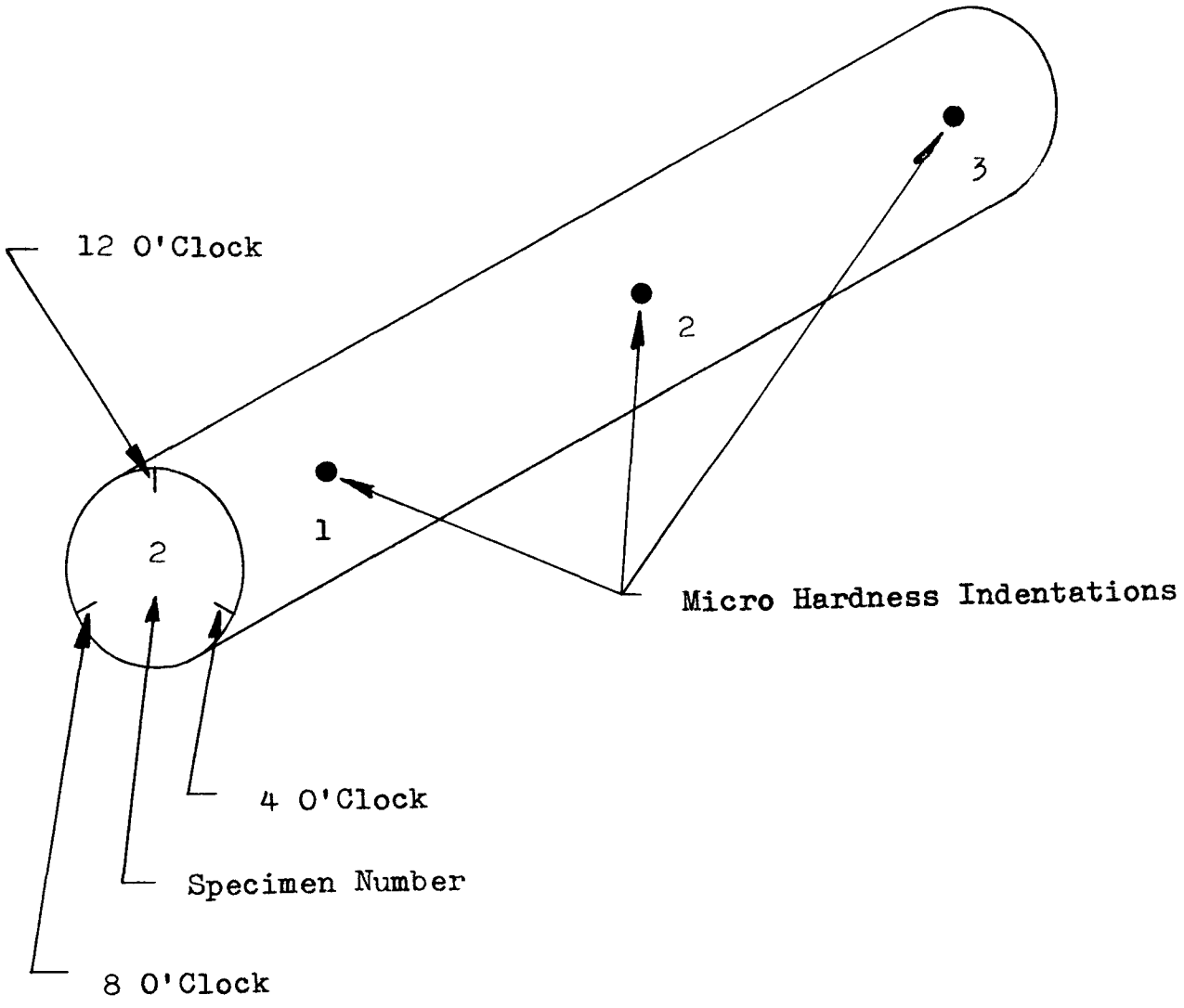

FIGURE 26

Bench Mark System Used To Index The Thermal Endurance Test Pellets

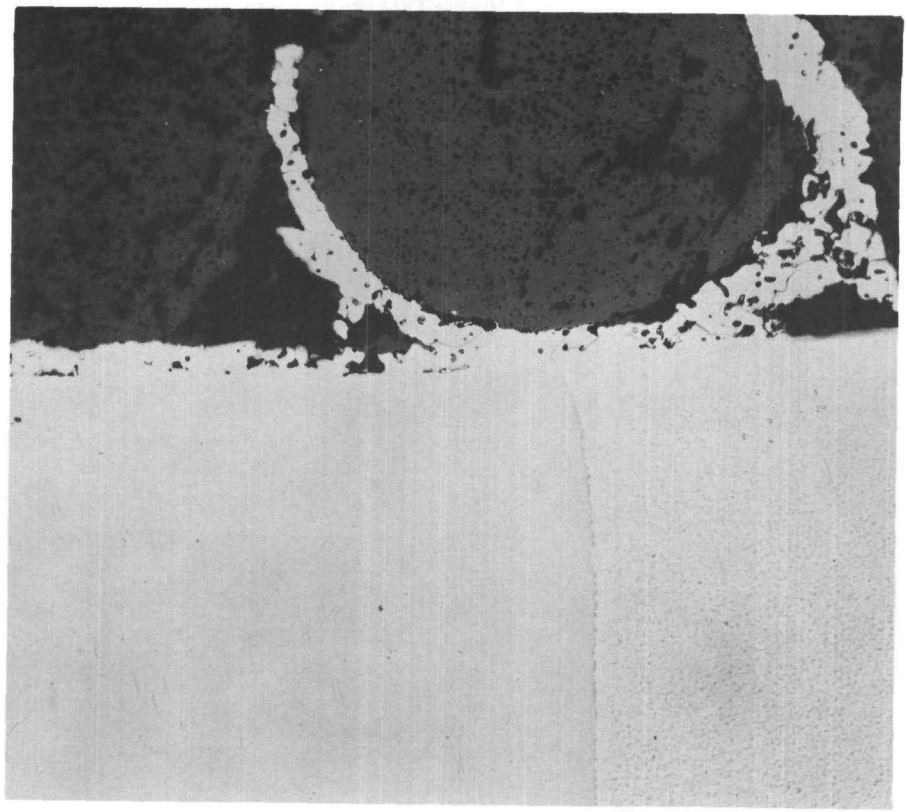

FIGURE 27

Fuel-cladding interface of specimen number 147-2, 500 hours exposure at 1340°C.

Magn: 250X
As polished

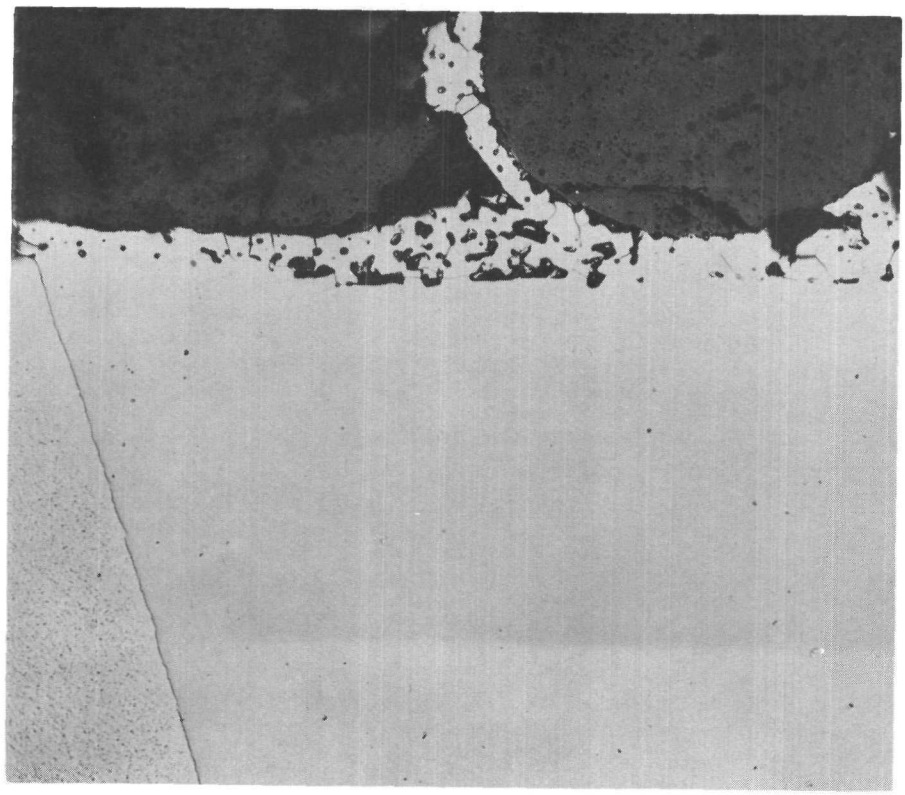

FIGURE 28

Fuel-cladding interface of specimen number 147-4, 500 hours exposure at 1400°C.

Magn: 250X
As polished

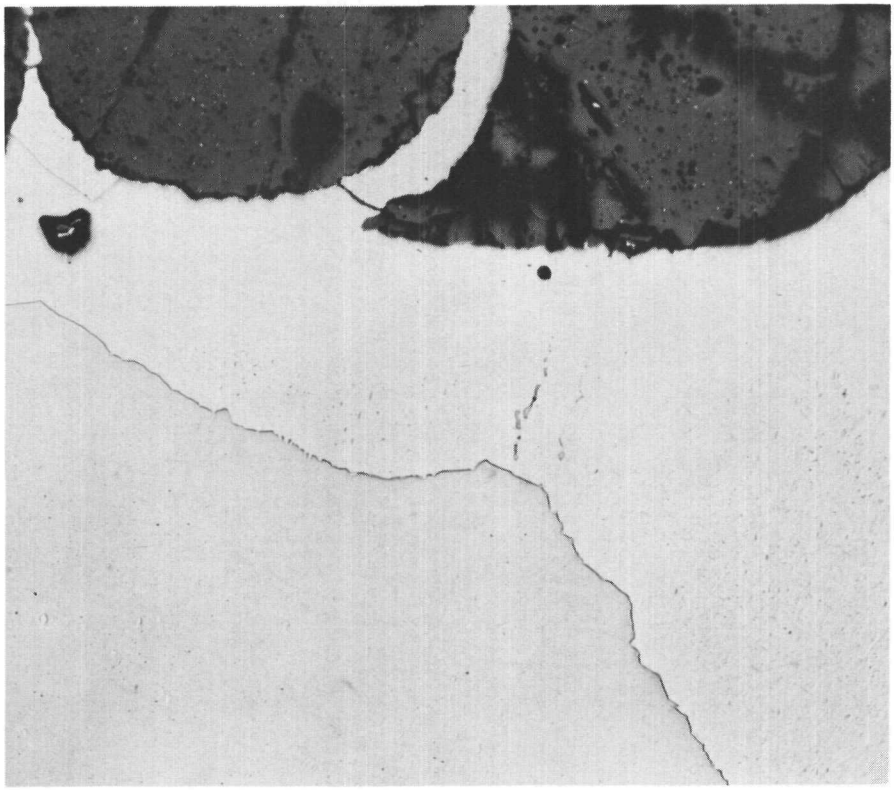

FIGURE 29

Fuel-cladding interface of specimen number 147-7, 500 hours exposure at 1450 to 1500°C.

Magn: 250X
As polished

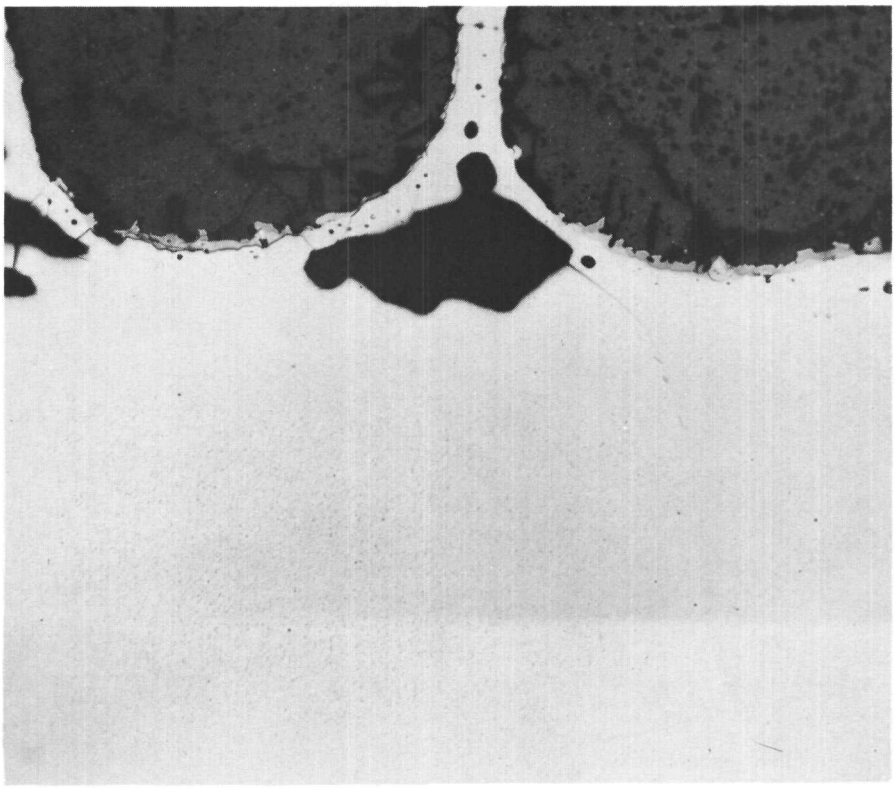

FIGURE 30

Fuel-cladding interface of specimen number 147-9, 500 hours exposure at 1450 to 1500°C.

Magn: 250X
As polished

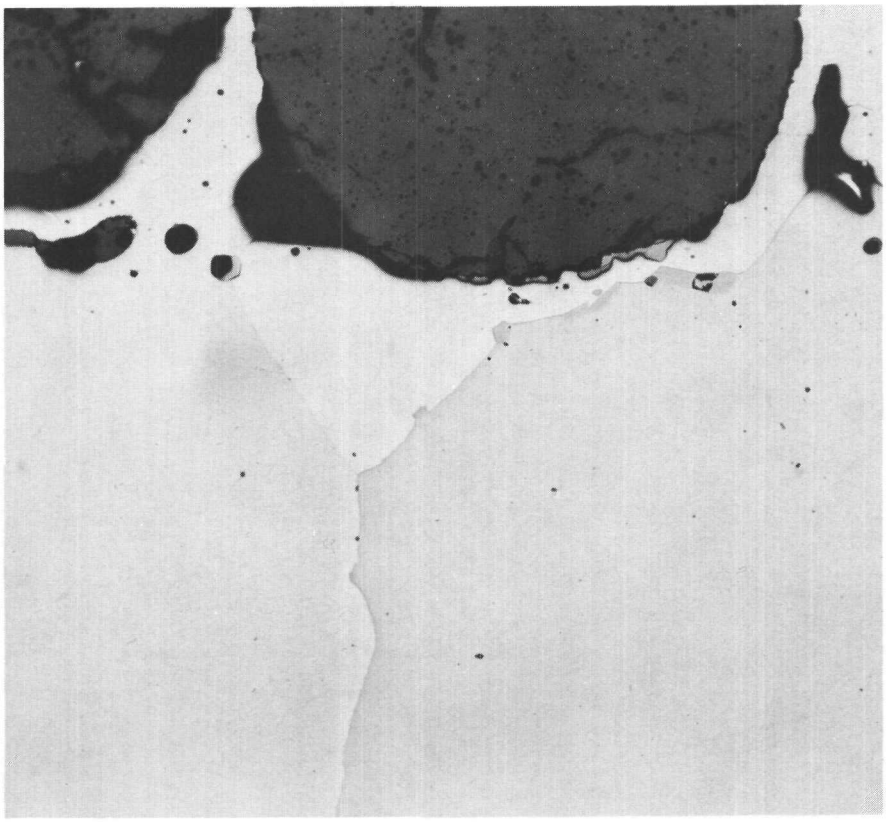

FIGURE 31

Fuel-cladding interface of specimen number 147-10, 500 hours exposure at 1500°C.

Magn: 250X
As polished

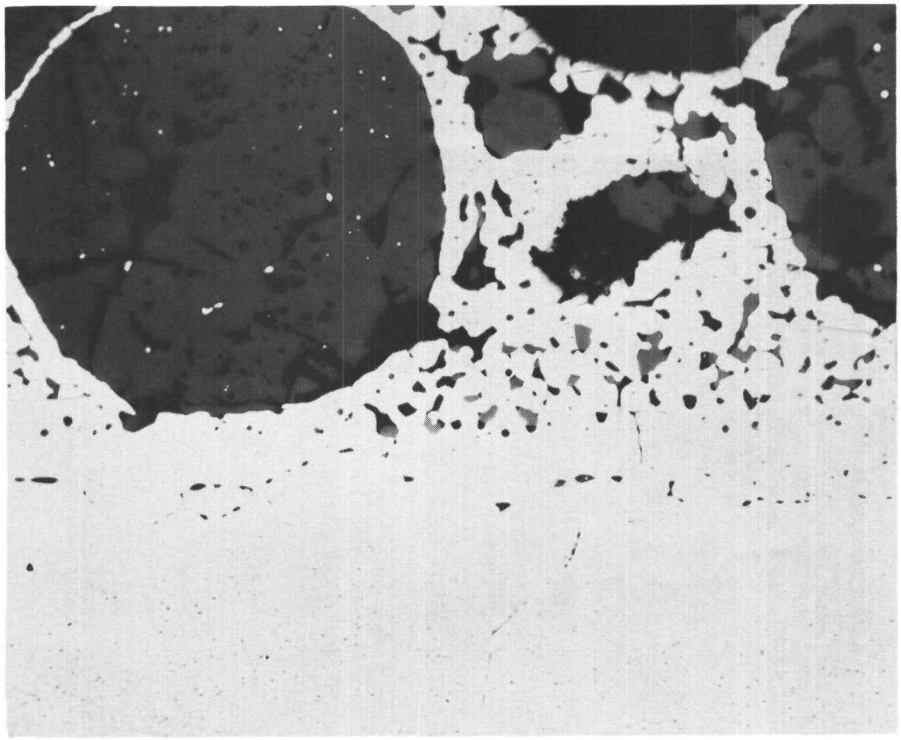

FIGURE 32

Fuel-cladding interface of thermal conductivity specimen number 1 showing the presence of intergranular diffusion. 500 hours exposure at 1550°C.

Magn: 250X
As polished

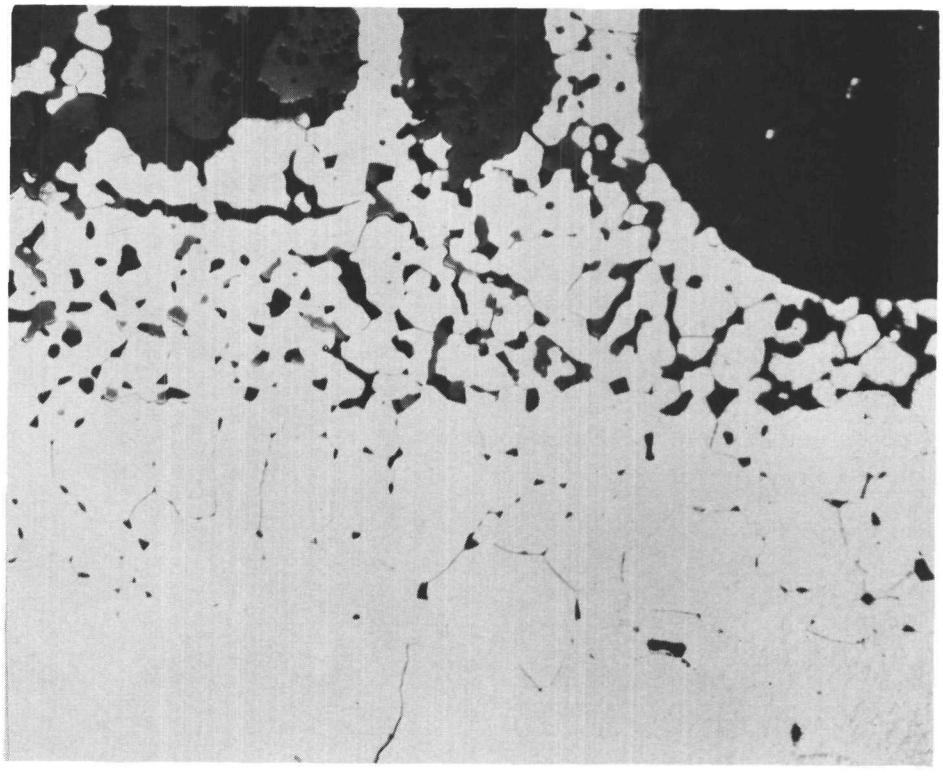

FIGURE 33

Fuel-cladding interface of thermal conductivity specimen number 2 showing the presence of intergranular diffusion. 500 hours exposure at 1550°C.

Magn: 250X As polished

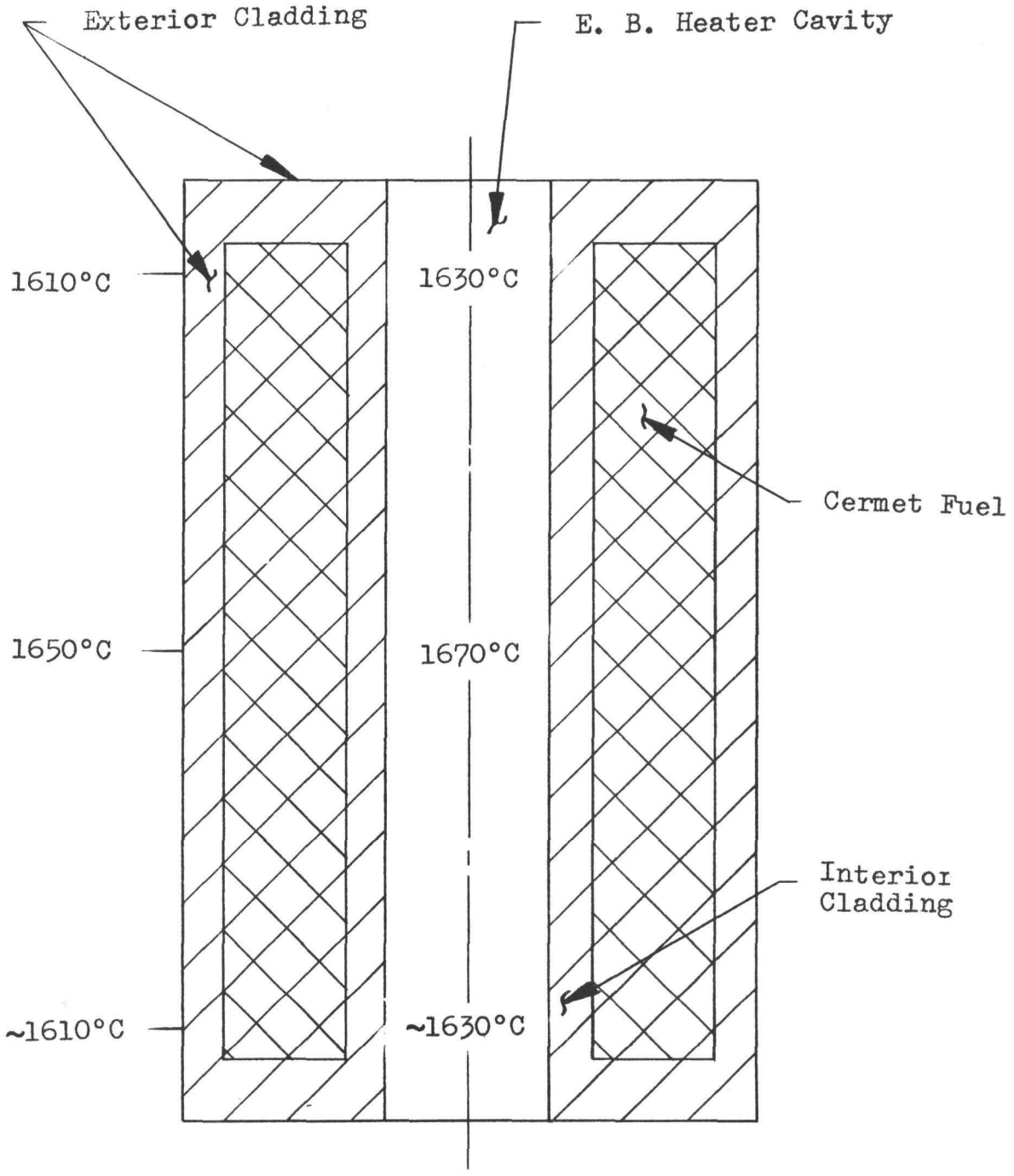

FIGURE 34

Temperature Profile Existing During Testing of
The Vacuum Emission Pellet.

DISTRIBUTION LIST

	Number of Copies
ASAPT Wright-Patterson Air Force Base, Ohio	1
ASAPR Wright-Patterson Air Force Base, Ohio	1
ASRMFP Wright-Patterson Air Force Base, Ohio	1
ASRPP-20 Attn: Lt. D. Raspet Static Energy Conversion Branch Flight Vehicle Power Division AF Aero Propulsion Laboratory Wright-Patterson Air Force Base, Ohio	3
ASRNET Wright-Patterson Air Force Base, Ohio	1
Office of Naval Research Code 429 Attn: Cmdr. John Connelly Washington 25, D.C.	1
AFCRL (CRZAP) L. G. Hanscom Field Bedford, Massachusetts	1
AFOSR (SRHPM) Attn: Dr. Milton Slawsky Building T-D Washington 25, D.C.	1
SSD (SSTRE, Capt. Evert) AF Unit Post Office Los Angeles 45, California	1
ASTIA (TIPDR) Arlington Hall Station Arlington 12, Virginia	21

	Number of Copies
U. S. Atomic Energy Commission Division of Reactor Development Attn: Cmdr. W. Schoenfeld Washington 25, D.C.	1
Advanced Research Products Agency Attn: Dr. John Huth Washington 25, D.C.	1
Jet Propulsion Laboratory Spacecraft Secondary Power Section Attn: Mr. Paul Goldsmith 4800 Oak Park Drive Pasadena, California	1
Aerospace Corporation Attn: Library Technical Document Group Post Office Box 95085 Los Angeles 45, California	1
NASA - Lewis Research Center SEPO Attn: Mr. R. Dennington 21000 Brookpark Road Cleveland 35, Ohio	1
U. S. Atomic Energy Commission San Francisco Operation Office 2111 Boncroft Way Attn: Reactor Division Berkeley 4, California	1
NASA Manned Spacecraft Center SEDD Attn: J. D. Murrell Houston, Texas	1
U. S. Atomic Energy Commission Office of Technical Information P.O. Box 62 Oak Ridge, Tennessee	1